GYOTO 2.0: a polarized relativistic ray-tracing code

N Aimar[1,2,3,6,*] ⓘ**, T Paumard**[1,6] ⓘ**, F H Vincent**[1,6] ⓘ**,
E Gourgoulhon**[4,5] ⓘ **and G Perrin**[1] ⓘ

[1] LESIA, Observatoire de Paris, CNRS, Université Pierre et Marie Curie, Université Paris Diderot, 5 place Jules Janssen, 92190 Meudon, France
[2] Faculdade de Engenharia da Universidade do Porto, s/n, R. Dr. Roberto Frias, Porto 4200-465, Portugal
[3] CENTRA, Departamento de Física, Instituto Superior Técnico-IST, Universidade de Lisboa-UL, Avenida Rovisco Pais 1, Lisboa 1049-001, Portugal
[4] Laboratoire Univers et Théories, Observatoire de Paris, CNRS, Université PSL, Université Paris Cité, 5 place Jules Janssen, 92190 Meudon, France
[5] Laboratoire de Mathématiques de Bretagne Atlantique, CNRS, Université de Bretagne Occidentale, 6 avenue Le Gorgeu, 29238 Brest, France

E-mail: nicolas.aimar64@gmail.com

Abstract

Polarized general-relativistic radiative transfer in the vicinity of black holes and other compact objects has become a crucial tool for probing the properties of relativistic astrophysics plasmas. Instruments like GRAVITY, the Event Horizon telescope, Atacama Large Millimeter/submillimeter Array, or Imaging x-ray Polarimetry Explorer make it very timely to develop such numerical frameworks. In this article, we present the polarized extension of the public ray-tracing code GYOTO, and offer a python notebook allowing to easily perform a first realistic computation. The code is very modular and allows to conveniently add extensions for the specific needs of the user. It is agnostic about the spacetime and can be used for arbitrary compact objects. We demonstrate the validity of the code by providing tests, and show in particular a perfect agreement with the IPOLE code. Our article also aims at pedagogically introducing all the relevant formalism in a self-contained manner.

Keywords: relativistic processes, radiative transfer, polarization, ray-tracing, black holes

---

1. Introduction

Generating synthetic images of black hole environments is tricky because of relativistic effects such as aberration, Doppler beaming, gravitational redshift and light bending. General-relativistic radiative transfer (GRRT) computation through ray-tracing method, i.e. integration of photons trajectories (null geodesics, assuming no impact other than gravitation on the trajectory), allows to naturally account for all relativistic effects to generate synthetic observables of such environments that can be compared to observational data. This technique is key to obtain meaningful constraints on the parameters describing the emitting accretion flow or the spacetime geometry. It can be used either on analytically described accretion flows, or in post-processing of general relativistic magnetohydrodynamical (GRMHD) simulations. For example, the Numerical Observatory of Violent Accreting system (NOVAs; Varniere *et al* 2018, Mignon-Risse *et al* 2021) combines GRMHD simulations of accretion flows around black holes as computed by the code GR-AMRVAC (Casse *et al* 2017), with the ray-tracing code GYOTO (Vincent *et al* 2011) to produce various synthetic observables.

The recent development of instruments now allows to measure the polarization of light coming from the extremely close environment of black holes. The Event Horizon Telescope (EHT) released the millimetric polarized image of M87* (Event Horizon Telescope Collaboration *et al* 2022). GRAVITY (GRAVITY Collaboration *et al* 2018, 2023) in the near infrared, and the Atacama Large Millimeter/submillimeter Array (ALMA, Wielgus *et al* 2022) have detected a polarized signature of the radiation flares associated with the supermassive black hole at the center of the Galaxy, Sagittarius A* (Sgr A*). Moreover, the Imaging x-ray Polarimetry Explorer (IXPE) has obtained important constraints on the geometry of the accretion flow of an x-ray binary by measuring its polarized radiation (Krawczynski *et al* 2022).

Thus, polarized ray-tracing codes are of particular interest to generate synthetic observables from accretion models, be they analytic (see e.g. Broderick *et al* 2016, Gralla *et al* 2018, 2019, 2020, Vincent *et al* 2019, GRAVITY Collaboration *et al* 2020, Nalewajko *et al* 2020, Dovčiak *et al* 2022, Vos *et al* 2022, Aimar *et al* 2023, Cárdenas-Avendaño and Lupsasca 2023), or numeric (see e.g. Chan *et al* 2015, Mościbrodzka *et al* 2016, Chael *et al* 2018, 2019, Davelaar *et al* 2018, Event Horizon Telescope Collaboration *et al* 2019, Anantua *et al* 2020, Dexter *et al* 2020, Porth *et al* 2021). In particular, polarization signatures might allow probing the nature of spacetime close to the event horizon of black hole candidates, making GRRT a crucial tool for constraining general relativity (GR) in the strong-field regime (Himwich *et al* 2020, Jiménez-Rosales *et al* 2021, Vincent *et al* 2023).

The need for ray tracing when computing images in GR led to the development of multiple codes. Many of them were developed for unpolarized light (Noble *et al* 2007, Dexter and Agol 2009, Dauser *et al* 2010, Vincent *et al* 2011, Pu *et al* 2016, Bronzwaer *et al* 2018, Chan *et al* 2018, Younsi *et al* 2020). Some codes also keep track of the electric vector position angle and polarization degree, assuming a geometrically thin equatorial accretion flow (Dovčiak *et al* 2008, Gelles *et al* 2021, Cárdenas-Avendaño *et al* 2023), the latter two being specialized for highly-lensed features by implementing adaptive ray tracing. Only a handful of codes are able of treating the most demanding problem of integrating the full polarized radiative transfer: GRTRANS (Dexter 2016), IPOLE (Mościbrodzka and Gammie 2018), ARCMANCER (Pihajoki *et al* 2018), BHOSS (Younsi *et al* 2020), RAPTOR (Bronzwaer *et al* 2020), BLACKLIGHT (White 2022), as well as LEMON (Xiao-lin *et al* 2021) which specializes on polarized radiative transfer with scattering. Some of these polarized GRRT codes were recently compared by Prather *et al* (2023).

GYOTO (Vincent *et al* 2011) is a backwards ray-tracing code (i.e. integrating from the observer to the source), operating in any given (analytically or numerically computed) metric, and solving the radiative transfer equation. It can also integrate timelike geodesics for computing e.g. stellar orbits (Grould *et al* 2017). The code is publicly available[7] , built to be modular so that extensions are easy to integrate and user-friendly with XML and python interfaces.

The goals of this paper are the following: (i) providing the new version of GYOTO, with full polarized GRRT included, publicly available at the same address as the older version, with the addition of a python snippet[8] to allow the interested reader to immediately be able to compute a non-trivial setup; (ii) providing a pedagogical, in-depth presentation of the formalism of GR polarization, as well as a detailed description of the technical implementation. In the following discussion, we will focus on polarized synchrotron radiation, as it is the dominant emission mechanism for our sources of primary scientific interest (Sgr A* and M87). But the code is able to compute polarized observables for other emission mechanism as soon as the electric field is provided in the model. Section 2 presents the formalism of GR polarized radiative transfer. In section 3, we present various tests that we made to validate our code. The last section is dedicated to discussion and conclusion.

2. Formalism

We will discuss the problem of polarized GRRT taking the usual point of view of ray tracing. We thus consider a light ray (mathematically speaking, a null geodesic) integrated backwards from a distant observer's screen towards some source of radiation. The problem can then be divided into three main parts that will be discussed hereafter:

- The definition of a wave vector at the distant observer's screen, tangent to the considered null geodesic, together with a pair of spacelike vectors forming an orthonormal basis of the observer's screen;
- The backwards parallel propagation along the considered null geodesic of the wave vector together with the screen basis, until a source of radiation is reached;
- The integration of polarized radiative transfer within the source.

Before describing these three steps in detail, we will start by providing important definitions in the next section.

2.1. Geometric optics, light ray, covariant and observer-specific polarization vectors

We consider a monochromatic plane electromagnetic wave propagating in a given spacetime. The geometrical optics approximation of Maxwell's equations under Lorenz gauge condition allows to describe this wave as follows.

The complex 4-potential 1-form reads

$$\hat{\mathbf{A}} = \hat{\mathbf{a}}\, e^{i\Phi}, \tag{1}$$

---

[7] https://github.com/gyoto/Gyoto/blob/master/INSTALL.Gyoto.md.
[8] https://github.com/gyoto/Gyoto/blob/master/doc/examples/Gyoto_Polar_example.ipynb.

where $\hat{\mathbf{a}}$ is the amplitude 1-form, assumed to vary much slower than the phase Φ (this is the basic idea of the geometrical optics approximation). The hat reminds that we are dealing with complex quantities. The Faraday electromagnetic 2-form,

$$\hat{\mathcal{F}} = \mathbf{d}\hat{\mathbf{A}}, \tag{2}$$

then reads in components

$$\begin{aligned}
\hat{\mathcal{F}}_{\alpha\beta} &= \nabla_\alpha \hat{A}_\beta - \nabla_\beta \hat{A}_\alpha \\
&= e^{i\Phi} \nabla_\alpha \hat{a}_\beta + \hat{a}_\beta\, i\, e^{i\Phi} \nabla_\alpha \Phi - \left(e^{i\Phi} \nabla_\beta \hat{a}_\alpha + \hat{a}_\alpha\, i\, e^{i\Phi} \nabla_\beta \Phi \right) \\
&\approx i \left(\hat{a}_\beta\, k_\alpha - \hat{a}_\alpha\, k_\beta \right) e^{i\Phi},
\end{aligned} \tag{3}$$

where we introduce the *wave vector*

$$\mathbf{k} \equiv \boldsymbol{\nabla}\Phi, \tag{4}$$

and use the geometric optics approximation to neglect the variations of the amplitude, i.e. the $\nabla_\alpha \hat{a}_\beta$ terms.

Plugging this into Maxwell's equations and assuming Lorenz gauge (that is, the divergence of $\hat{\mathbf{A}}$ should vanish) leads to the following results:

- $\mathbf{k}$ is a null vector parallel propagated along itself,

$$\mathbf{k} \cdot \mathbf{k} = 0, \quad \boldsymbol{\nabla}_{\mathbf{k}} \mathbf{k} = \mathbf{0}, \tag{5}$$

so that it defines a null geodesic, which we define as a *light ray*;
- We can introduce the unit spacelike *covariant polarization vector*

$$\hat{\mathbf{f}} \equiv \frac{\hat{\mathbf{a}}}{a}, \tag{6}$$

where $\hat{\mathbf{a}}$ is the complex vector corresponding to the amplitude 1-form introduced in equation (1) by metric duality (we use the same notation for both quantities in order to simplify the notation). The scalar quantity a is the modulus of the complex vector $\hat{\mathbf{a}}$,

$$a = \sqrt{\hat{a}_\mu \hat{a}^{\mu*}}. \tag{7}$$

Our naming convention specifies that this vector is covariant in order to differentiate it from the polarization vector as observed by a specific observer, which will be our quantity of prime interest in the following. The covariant polarization vector satisfies the two following important properties: (i) it is perpendicular to the wave vector $\mathbf{k}$ (this is a consequence of the Lorenz gauge choice), and (ii) it is parallel transported along $\mathbf{k}$ in vacuum (this is a consequence of Maxwell's equations):

$$\hat{\mathbf{f}} \cdot \mathbf{k} = 0, \quad \boldsymbol{\nabla}_{\mathbf{k}} \hat{\mathbf{f}} = \mathbf{0}. \tag{8}$$

We can thus reexpress the Faraday tensor in terms of the polarization and wave vectors as follows

$$\hat{\mathcal{F}}_{\alpha\beta} = i a \left(\hat{f}_\beta\, k_\alpha - \hat{f}_\alpha\, k_\beta \right) e^{i\Phi}. \tag{9}$$

From this expression we deduce the important property that it is possible to add any multiple of the wave vector $\mathbf{k}$ to the polarization vector $\hat{\mathbf{f}}$ without altering the Faraday tensor. So the polarization vector can be arbitrarily transformed under

$$\hat{\mathbf{f}} \mapsto \hat{\mathbf{f}} + q\mathbf{k} \tag{10}$$

for any scalar field q (note that q is not necessarily a constant, it is an arbitrary scalar field).

So far, we have only used global quantities that are not defined with respect to any particular observer. We now want to introduce the electric and magnetic fields as observed by the distant observer, $\mathcal{O}$, the oscillations of which define the observed electromagnetic wave. Let us denote by $\mathbf{u_0}$ the 4-velocity of observer $\mathcal{O}$. By definition, the electric linear form and the magnetic vector as measured by a generic observer with 4-velocity $\mathbf{u}$ read[9]

$$\hat{E}_\alpha = \hat{\mathcal{F}}_{\alpha\mu} u^\mu,$$
$$\hat{B}^\alpha = -\frac{1}{2}\epsilon^{\alpha\mu\nu}{}_\rho \hat{\mathcal{F}}_{\mu\nu} u^\rho, \tag{11}$$

where ϵ is the Levi-Civita tensor. The electric field vector $\hat{\mathbf{E}}_\mathbf{0}$ as observed by the distant observer $\mathcal{O}$ thus reads

$$
\begin{aligned}
\hat{E}^\rho &= g^{\rho\alpha} \hat{E}_\alpha \\
&= g^{\rho\alpha} \hat{\mathcal{F}}_{\alpha\beta} u^\beta \\
&= i a e^{i\Phi} g^{\rho\alpha} \left(\hat{f}_\beta k_\alpha - \hat{f}_\alpha k_\beta\right) u^\beta \\
&= i a e^{i\Phi} \left(\hat{f}_\beta k^\rho - \hat{f}^\rho k_\beta\right) u^\beta \\
&= i a e^{i\Phi} \left(\left(\hat{\mathbf{f}}_\mathbf{0} \cdot \mathbf{u_0}\right) k^\rho + \omega_\mathbf{0}\hat{f}^\rho\right),
\end{aligned}
\tag{12}
$$

where we drop the lower index 0 for the components of the various tensors for simplicity (all of them being evaluated at the distant observer's location), and we introduce $\omega_\mathbf{0} \equiv -\mathbf{k_0} \cdot \mathbf{u_0}$, where $\mathbf{k_0}$ is the wave vector at the distant observer's location. This quantity ω_0 is the pulsation of the photon as measured by $\mathcal{O}$. All vectors with a lower index 0 are defined at the distant observer's screen.

Let us decompose the vectors $\hat{\mathbf{f}}_\mathbf{0}$ and $\mathbf{k_0}$ in parts parallel and orthogonal to the observer's 4-velocity:

$$
\begin{aligned}
\mathbf{k_0} &= \omega_\mathbf{0} \mathbf{u_0} + \mathbf{K_0}, & \mathbf{K_0} &\perp \mathbf{u_0}, \\
\hat{\mathbf{f}}_\mathbf{0} &= -\left(\hat{\mathbf{f}}_\mathbf{0} \cdot \mathbf{u_0}\right) \mathbf{u_0} + \hat{\mathbf{f}}_\mathbf{0}^\perp, & \hat{\mathbf{f}}_\mathbf{0}^\perp &\perp \mathbf{u_0}.
\end{aligned}
\tag{13}
$$

Note that

$$\hat{\mathbf{f}}_\mathbf{0}^\perp \cdot \hat{\mathbf{f}}_\mathbf{0}^\perp = 1 + \left(\hat{\mathbf{f}}_\mathbf{0} \cdot \mathbf{u_0}\right)^2 \tag{14}$$

---

[9] We highlight that the electric and magnetic fields discussed here are the electromagnetic fields describing the monochromatic wave that reaches the observer's screen. They should not be confused with the electromagnetic fields that might exist at the source location, for instance the magnetic field of the accretion flow surrounding the black hole.

so that $\hat{\mathbf{f}}_0^\perp$ is not a unit vector in general. It is normalized only if $\hat{\mathbf{f}}_0 \cdot \mathbf{u}_0 = 0$, in which case we simply have $\hat{\mathbf{f}}_0^\perp = \hat{\mathbf{f}}_0$. Similary, $\mathbf{K}_0$ is not a unit vector and it is easy to show that

$$\mathbf{K}_0 \cdot \mathbf{K}_0 = \omega_0^2. \tag{15}$$

The vector $\mathbf{K}_0$ coincides with the incident wave vector as measured by observer $\mathcal{O}$.

In terms of the vectors normal to $\mathbf{u}_0$ we immediately obtain the final expression of the electric vector as observed by $\mathcal{O}$:

$$\hat{\mathbf{E}}_0 = i\,a\,e^{i\Phi} \left(\omega_0 \hat{\mathbf{f}}_0^\perp - \frac{\mathbf{K}_0 \cdot \hat{\mathbf{f}}_0^\perp}{\omega_0} \mathbf{K}_0 \right). \tag{16}$$

This vector is clearly orthogonal to the direction of propagation $\mathbf{K}_0$, and it is also orthogonal to the 4-velocity $\mathbf{u}_0$, as it should for a vector living in the local rest space of the observer.

Then, the magnetic field vector $\hat{\mathbf{B}}_0$ as observed by $\mathcal{O}$ reads

$$\begin{aligned}
\hat{B}^\rho &= -\frac{1}{2}\,\epsilon^{\rho\mu\nu}{}_\alpha \hat{\mathcal{F}}_{\mu\nu} u^\alpha \\
&= -\frac{1}{2} i\,a\,e^{i\Phi}\,\epsilon^{\rho\mu\nu}{}_\alpha \left(\hat{f}_\nu k_\mu - \hat{f}_\mu k_\nu \right) u^\alpha \\
&= -i\,a\,e^{i\Phi}\,\epsilon^{\rho\mu\nu}{}_\alpha \hat{f}_\nu k_\mu u^\alpha \\
&= -i\,a\,e^{i\Phi}\,\epsilon^\rho{}_{\mu\nu\alpha} u^\alpha k^\mu \hat{f}^\nu \\
&= i\,a\,e^{i\Phi}\,\epsilon_{\alpha\mu\nu}{}^\rho u^\alpha k^\mu \hat{f}^\nu \\
&= i\,a\,e^{i\Phi}\,\epsilon_{\alpha\mu\nu}{}^\rho u^\alpha K^\mu \hat{f}^{\perp\nu},
\end{aligned} \tag{17}$$

where we have used extensively the antisymmetric nature of the Levi-Civita tensor. The last expression exactly coincides with the definition of the cross product in the vector space orthogonal to $\mathbf{u}_0$ (which we label by $\times_{\mathbf{u}_0}$), such that finally the magnetic field vector as measured by $\mathcal{O}$ reads

$$\hat{\mathbf{B}}_0 = i\,a\,e^{i\Phi}\,\mathbf{K}_0 \times_{\mathbf{u}_0} \hat{\mathbf{f}}_0^\perp. \tag{18}$$

This vector is also obviously orthogonal to the direction of propagation $\mathbf{K}_0$, and to the electric vector.

We can now define the notion of *polarization vector as measured by observer $\mathcal{O}$*:

$$\hat{\mathbf{F}}_0 = \mathbf{K}_0 \times_{\mathbf{u}_0} \hat{\mathbf{B}}_0, \tag{19}$$

which is by construction normal to the direction of propagation and to the magnetic field vector. We note that this quantity depends on the observer, just as the electric and magnetic fields, while the covariant polarization vector $\hat{\mathbf{f}}_0$, defined in equation (6), is a covariant quantity. They obviously differ given that by construction $\hat{\mathbf{F}}_0$ is orthogonal to the observer's 4-velocity $\mathbf{u}_0$, while $\hat{\mathbf{f}}_0$ is defined independently from $\mathbf{u}_0$. A natural question is to investigate the relation between $\hat{\mathbf{F}}_0$ and $\hat{\mathbf{f}}_0^\perp$ that both live in the vector space orthogonal to $\mathbf{u}_0$. These two vectors are completely independent *a priori*, because $\hat{\mathbf{F}}_0$ is by construction orthogonal to both $\mathbf{K}_0$ and $\hat{\mathbf{B}}_0$ (see equation (19)), while $\hat{\mathbf{f}}_0^\perp$ is only orthogonal to $\hat{\mathbf{B}}_0$ (see equation (18)), but not to $\mathbf{K}_0$. Indeed, from equations (8) and (13), we have

$$\hat{\mathbf{f}}_\mathbf{0} \cdot \mathbf{k_0} = 0$$

$$\Leftrightarrow \left(\hat{\mathbf{f}}_\mathbf{0} \cdot \mathbf{u_0}\right) \omega_\mathbf{0} + \hat{\mathbf{f}}_\mathbf{0}^\perp \cdot \mathbf{K_0} = 0 \tag{20}$$

so that only if $\hat{\mathbf{f}}_\mathbf{0} \cdot \mathbf{u_0} = 0$ (which has no reason to hold in general) is $\hat{\mathbf{f}}_\mathbf{0}^\perp$ orthogonal to $\mathbf{K_0}$. In this special case, we saw in equation (13) that $\hat{\mathbf{f}}_\mathbf{0}^\perp = \hat{\mathbf{f}}_\mathbf{0}$, so that when $\hat{\mathbf{f}}_\mathbf{0} \cdot \mathbf{u_0} = 0$, and only then, $\hat{\mathbf{f}}_\mathbf{0}$ is the unit vector along $\hat{\mathbf{F}}_\mathbf{0}$. However, we have seen in equation (10) that the covariant polarization vector is defined up to a term proportional to the wavevector, the proportionality coefficient being a scalar field. We can thus choose to work with a covariant polarization vector $\mathbf{f}'$ such that, at the distant observer's location

$$\hat{\mathbf{f}}_\mathbf{0}' = \hat{\mathbf{f}}_\mathbf{0} + \frac{\hat{\mathbf{f}}_\mathbf{0} \cdot \mathbf{u_0}}{\omega_\mathbf{0}} \mathbf{k_0}. \tag{21}$$

This vector is such that

$$\hat{\mathbf{f}}_\mathbf{0}' \cdot \mathbf{u_0} = 0, \tag{22}$$

and we saw just above that this implies that $\hat{\mathbf{f}}_\mathbf{0}'$ is then the unit vector along $\hat{\mathbf{F}}_\mathbf{0}$. Thanks to the degree of liberty in the definition of the covariant polarization vector expressed by equation (10), we can thus confuse the covariant and non-covariant polarization vectors at the observer, $\hat{\mathbf{f}}_\mathbf{0}$ and $\hat{\mathbf{F}}_\mathbf{0}$.

By virtue of the double vector product law we have

$$\left(\mathbf{K_0} \times_{\mathbf{u_0}} \hat{\mathbf{B}}_\mathbf{0}\right)^\alpha = i\, a\, e^{i\phi} \left[\left(\mathbf{K_0} \cdot \hat{\mathbf{f}}_\mathbf{0}^\perp\right) K^\alpha - (\mathbf{K_0} \cdot \mathbf{K_0}) \hat{f}^{\perp\,\alpha}\right]$$

$$= i\, a\, e^{i\phi} \omega_\mathbf{0} \left[\frac{\mathbf{K_0} \cdot \hat{\mathbf{f}}_\mathbf{0}^\perp}{\omega_\mathbf{0}} K^\alpha - \omega_\mathbf{0} \hat{f}^{\perp\,\alpha}\right] \tag{23}$$

so that finally

$$\hat{\mathbf{F}}_\mathbf{0} = \left(\mathbf{K_0} \times_{\mathbf{u_0}} \hat{\mathbf{B}}_\mathbf{0}\right) = -\omega_\mathbf{0} \hat{\mathbf{E}}_\mathbf{0}. \tag{24}$$

We thus conclude that the polarization vector as measured by $\mathcal{O}$ coincides, up to a normalization factor, with the electric field as measured by $\mathcal{O}$. The various vectors lying in observer $\mathcal{O}$'s local rest space (that is, the vector space orthogonal to the 4-velocity $\mathbf{u_0}$) are depicted in figure 1. We introduce in this figure the *electric vector position angle* (EVPA), defined in the local frame of the distant observer, which is the angle between a reference direction (the local North of the distant observer) and the polarization vector $\hat{\mathbf{F}}_\mathbf{0}$.

2.2. Polarization basis defined at the distant observer's screen

We take here the typical point of view of a ray-tracing problem where the initial conditions are fixed at the far-away observer's screen, and the integration is performed backwards in time from the screen towards the source. This allows to save a lot of computing time by integrating only those geodesics that will approach the source by shooting light rays only within a small solid angle subtending the source. The aim of this subsection is to explicitly describe our initial conditions at the observer's screen, which is illustrated in figure 2. In order to be specific, we will consider a black hole spacetime, but the discussion is very general and is not restricted to this particular case.
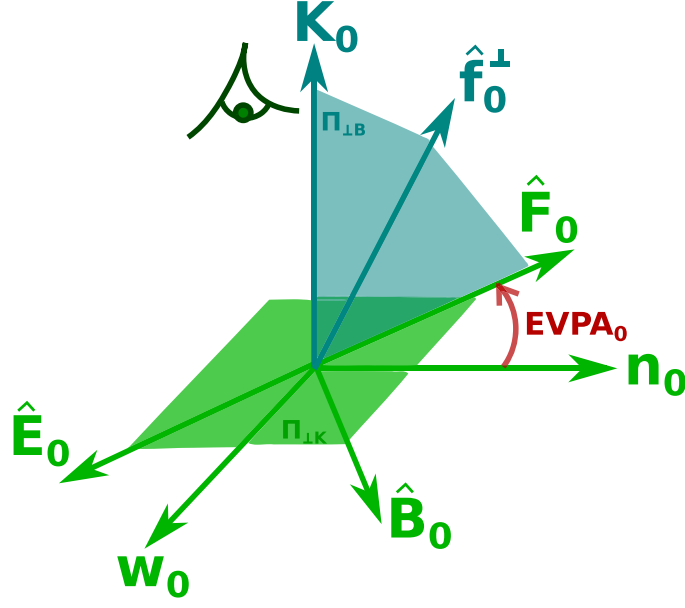
Figure 1. Vectors lying in the distant observer $\mathcal{O}$'s local rest space (the vector space orthogonal to $\mathcal{O}$'s 4-velocity $\mathbf{u_0}$). $\mathbf{K_0}$ is the wave vector projected orthogonal to $\mathbf{u_0}$. The vectors $\bar{\mathbf{w}}_\mathbf{0}$ and $\bar{\mathbf{n}}_\mathbf{0}$ are unit vectors pointing towards the local West and North directions, so that $(\mathbf{K_0}, \bar{\mathbf{w}}_\mathbf{0}, \bar{\mathbf{n}}_\mathbf{0})$ forms a direct orthogonal triad. $\hat{\mathbf{E}}_\mathbf{0}$ and $\hat{\mathbf{B}}_\mathbf{0}$ are the electric and magnetic vectors as measured by $\mathcal{O}$, associated with the incident light wave, so that $(\mathbf{K_0}, \hat{\mathbf{E}}_\mathbf{0}, \hat{\mathbf{B}}_\mathbf{0})$ is a direct orthogonal triad. $\hat{\mathbf{F}}_\mathbf{0}$ is the polarization vector as measured by $\mathcal{O}$ (defined in equation (19)), which is antiparallel to $\hat{\mathbf{E}}_\mathbf{0}$ as stated by equation (24). $\hat{\mathbf{f}}_\mathbf{0}^\perp$ is the covariant polarization vector (defined in equation (6)) projected orthogonal to $\mathbf{u_0}$. The plane orthogonal to $\mathbf{K_0}$ (observer's screen plane) is drawn in green. It contains the electric and magnetic field vectors, and the polarization vector as measured by $\mathcal{O}$. The plane orthogonal to $\hat{\mathbf{B}}_\mathbf{0}$ is drawn in blue-green. It contains the photon's wave vector $\mathbf{K_0}$, the electric vector $\hat{\mathbf{E}}_\mathbf{0}$, and both the covariant and $\mathcal{O}$'s specific polarization vectors. The observed Electric Vector Position Angle (EVPA$_0$), measured East of North in the screen's plane, is shown in dark red.

The observer's screen is considered to be a pin-hole camera, with the various pixels corresponding to different directions on sky. The local rest space of the observer is spanned by a direct orthonormal triad $(\bar{\mathbf{e}}_1, \bar{\mathbf{e}}_2, \bar{\mathbf{e}}_3)$. Here and in the following, a bar on top of a vector denotes a spacelike unit vector. The vector $\bar{\mathbf{e}}_3$ is along the line of sight, normal to the screen, towards the black hole. If we consider spherical coordinates centered on the black hole (e.g. Boyer–Lindquist coordinates) and a direct orthonormal triad $(\bar{\mathbf{e}}_r, \bar{\mathbf{e}}_\theta, \bar{\mathbf{e}}_\varphi)$ associated with these coordinates, then $\bar{\mathbf{e}}_3 = -\bar{\mathbf{e}}_r$. The screen's plane is spanned by $(\bar{\mathbf{e}}_1, \bar{\mathbf{e}}_2)$, and we consider the special case $\bar{\mathbf{e}}_2 = -\bar{\mathbf{e}}_\theta$, which boils down to assuming that the projection of the black hole's angular momentum on the screen is along $\bar{\mathbf{e}}_2$. For a $N \times N$ pixels screen, one pixel with indices (i, j), with $i, j = 1 \ldots N$, corresponds to a pair of equatorial angles (see figure 2)

$$\alpha = \frac{f}{N}\left(i - \frac{N+1}{2}\right),$$
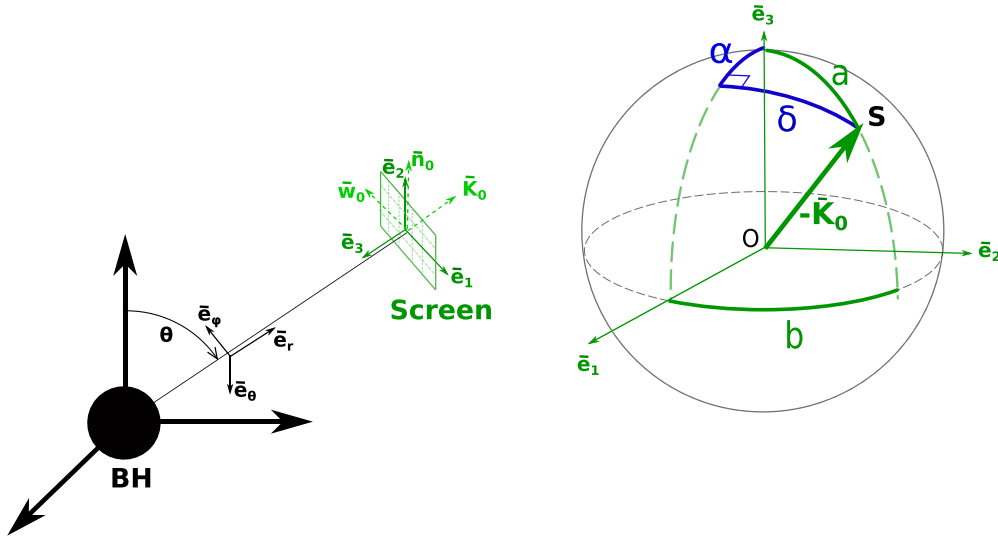$$\delta = \frac{f}{N}\left(j - \frac{N+1}{2}\right), \tag{25}$$

Figure 2. Initial condition of the polarized ray-tracing problem at the distant observer's screen. Left: A black hole (BH) spacetime is represented for being specific, but the figure is very general and applies to any kind of spacetime. We consider spherical coordinates and the spacelike orthonormal basis associated with these coordinates are labeled $(\bar{\mathbf{e}}_r, \bar{\mathbf{e}}_\theta, \bar{\mathbf{e}}_\varphi)$. The observer's local rest space is described by a direct orthonormal triad, $(\bar{\mathbf{e}}_1, \bar{\mathbf{e}}_2, \bar{\mathbf{e}}_3)$, where $\bar{\mathbf{e}}_3 = -\bar{\mathbf{e}}_r$, and where the screen's plane is contained in $\mathrm{Span}(\bar{\mathbf{e}}_1, \bar{\mathbf{e}}_2)$. We consider here that the 'upwards' direction of the observer's screen coincides with the projection of the black hole's angular momentum on the screen, i.e. that $\bar{\mathbf{e}}_2 = -\bar{\mathbf{e}}_\theta$. The unit direction of photon reception at the observer's screen is $\bar{\mathbf{K}}_\mathbf{0}$. The local polarization basis at the observer's screen, $(\bar{\mathbf{K}}_\mathbf{0}, \bar{\mathbf{w}}_\mathbf{0}, \bar{\mathbf{n}}_\mathbf{0})$, is shown, and corresponds to the central pixel of the screen, that is, to the purely radial incoming direction of the photon. Right: zoom on the local rest space $(\bar{\mathbf{e}}_1, \bar{\mathbf{e}}_2, \bar{\mathbf{e}}_3)$ and local celestial sphere of the observer. For a source of radiation located at S on the local celestial sphere, the unit direction of incidence is $\bar{\mathbf{K}}_\mathbf{0}$ (it is $-\bar{\mathbf{K}}_\mathbf{0}$ on the figure because $\bar{\mathbf{e}}_3$ points towards the source, while the incidence direction is of course in the opposite direction). The vector $\bar{\mathbf{K}}_\mathbf{0}$ is here not purely along the radial direction $\bar{\mathbf{e}}_3$ (in contrast with the left panel): it thus corresponds to a pixel that is not located at the center of the screen. The corresponding equatorial angles labeling the source, (α, δ), are shown, together with the corresponding spherical angles on the observer local sky, (a, b). For typical ray-tracing problems where the observer is far away, we have $a \ll 1$.

where f is the field of view of the observer. The corresponding spherical angles (see figure 2) on the local sky of the observer are given by standard spherical trigonometry relations:

$$\cos a = \cos \alpha \cos \delta,$$
$$\tan b = \frac{\tan \alpha}{\sin \delta}. \qquad (26)$$

The local unit direction of photon incidence then reads

$$\bar{\mathbf{K}}_\mathbf{0} = -\sin a \cos b\, \bar{\boldsymbol{e}}_\mathbf{1} - \sin a \sin b\, \bar{\boldsymbol{e}}_\mathbf{2} - \cos a\, \bar{\boldsymbol{e}}_\mathbf{3}$$
$$= \frac{\cos a}{\sqrt{g_{rr}}}\, \boldsymbol{\partial}_r + \frac{\sin a \sin b}{\sqrt{g_{\theta\theta}}}\, \boldsymbol{\partial}_\theta + \frac{\sin a \cos b}{\sqrt{g_{\varphi\varphi}}}\, \boldsymbol{\partial}_\varphi, \qquad (27)$$

where we have used the relations

$$\bar{\mathbf{e}}_r = \frac{\partial_r}{\sqrt{g_{rr}}}, \quad \bar{\mathbf{e}}_\theta = \frac{\partial_\theta}{\sqrt{g_{\theta\theta}}}, \quad \bar{\mathbf{e}}_\varphi = \frac{\partial_\varphi}{\sqrt{g_{\varphi\varphi}}}, \tag{28}$$

where ∂_i are spherical coordinate basis vectors, and $g_{ii} = \partial_i \cdot \partial_i$ are the corresponding metric coefficients. The null 4-vector tangent to the null geodesic when incident on the observer's screen then reads

$$\mathbf{k_0} = \partial_t + \bar{\mathbf{K}}_0, \tag{29}$$

where we consider that the observer's 4-velocity is $\mathbf{u_0} = \partial_t$ (assuming a static observer, and that $g_{tt} \to -1$ at the observer's location) and where we have assumed that $-\mathbf{k_0} \cdot \mathbf{u_0} = 1$, so that the spacelike vector $\bar{\mathbf{K}}_0$ in the last equation is normalized. This last assumption means that the photon's energy as measured by the far-away observer is unity, which does not change anything to the problem, it simply scales the energy, and physical values of energies can be easily retrieved when radiative transfer calculations are performed.

Once the photon arrival direction $\bar{\mathbf{K}}_0$ has been defined, it must be completed by two other vectors to form the local orthonormal polarization basis $(\bar{\mathbf{K}}_0, \bar{\mathbf{w}}_0, \bar{\mathbf{n}}_0)$. The vector $\bar{\mathbf{K}}_0$ corresponding to the central pixel of the screen coincides with a purely radial direction of arrival, $\bar{\mathbf{K}}_0^{\mathrm{cen}} = -\bar{\mathbf{e}}_3$ (the superscript 'cen' refers to the central pixel of the screen), see the left panel of figure 2. This particular vector can be easily completed by $\bar{\mathbf{w}}_0^{\mathrm{cen}} = -\bar{\mathbf{e}}_1$ and $\bar{\mathbf{n}}_0^{\mathrm{cen}} = \bar{\mathbf{e}}_2$, see the left panel of figure 2. In the general case of a vector $\bar{\mathbf{K}}_0$ defined by the two spherical angles (a, b) (see the right panel of figure 2), appendix A shows that the observer's screen polarization basis reads

$$\bar{\mathbf{w}}_0 = \left[-\sin^2 b \,(1 - \cos a) - \cos a \right] \bar{\mathbf{e}}_1 + \sin b \cos b \,(1 - \cos a) \bar{\mathbf{e}}_2 + \cos b \sin a \,\bar{\mathbf{e}}_3,$$
$$\bar{\mathbf{n}}_0 = -\sin b \cos b \,(1 - \cos a) \bar{\mathbf{e}}_1 + \left[\cos^2 b \,(1 - \cos a) + \cos a \right] \bar{\mathbf{e}}_2 - \sin b \sin a \,\bar{\mathbf{e}}_3. \tag{30}$$

It is straightforward to check that these vectors are unit vectors, orthogonal to each other, and to $\bar{\mathbf{K}}_0$. Moreover, in a typical ray-tracing problem where $a \ll 1$, we have as we should $\bar{\mathbf{w}}_0 \approx \bar{\mathbf{w}}_0^{\mathrm{cen}} = -\bar{\mathbf{e}}_1$, and $\bar{\mathbf{n}}_0 \approx \bar{\mathbf{n}}_0^{\mathrm{cen}} = \bar{\mathbf{e}}_2$. We note that the plane $(\bar{\mathbf{w}}_0, \bar{\mathbf{n}}_0)$ (where the polarization angle will be defined) strictly speaking only coincides with the screen's plane $(\bar{\mathbf{e}}_1, \bar{\mathbf{e}}_2)$ for the central pixel of the screen (with $a = 0$). We will neglect this small difference between the polarization plane and the screen's plane, which is perfectly valid as long as $a \ll 1$, that is, as long as the field of view is sufficiently small.

At this point, we have fully defined our initial condition by specifying the triad $(\mathbf{k_0}, \bar{\mathbf{w}}_0, \bar{\mathbf{n}}_0)$ at the observer's screen. The next step is to parallel transport these vectors along the light ray towards the source.

2.3. Relevant frames, parallel transport of polarization basis, EVPA

Let us start by introducing the three relevant frames for describing the polarized GRRT problem. We will focus on synchrotron radiation, which is our primary science interest, but most of the discussion is rather general. The frames of interest are:

- The *observer frame*, described in detail in the previous section, defined by the 4-velocity $\mathbf{u_0}$,
- The *fluid frame*, defined by the 4-velocity $\mathbf{u}$ describing the bulk motion of the emitting fluid (for instance, Keplerian motion around a black hole),
- The *particle frame*, which follows the helical motion of the synchrotron-emitting electron around the magnetic field lines described in the fluid frame.

This section will mostly deal with the fluid frame, and the link with the particle frame is further discussed in appendix B.

We consider a light ray, modeled by a null geodesic, joining the far-away observer to the emitting accretion flow surrounding a black hole. We want to parallel-transport the null 4-vector **k** tangent to the null geodesic, backwards from the observer towards the emitter. We will also parallel-transport the local West and North unit spacelike directions, $\bar{\mathbf{w}}$ and $\bar{\mathbf{n}}$. Note that the index 0 used for these three vectors in the previous section meant that they were considered at the screen position. We now consider their evolution along the ray and drop the index. So we must integrate the following equations

$$\nabla_{\mathbf{k}}\mathbf{k} = \mathbf{0},$$
$$\nabla_{\mathbf{k}}\bar{\mathbf{w}} = \mathbf{0},$$
$$\nabla_{\mathbf{k}}\bar{\mathbf{n}} = \mathbf{0}, \tag{31}$$

with the initial conditions that $(\mathbf{k}, \bar{\mathbf{w}}, \bar{\mathbf{n}}) = (\mathbf{k_0}, \bar{\mathbf{w}_0}, \bar{\mathbf{n}_0})$ at the screen. The integration is solved by means of a Runge–Kutta–Fehlberg algorithm of seventh order with an error estimator of order eight (RKF78), with an adaptive step. The absolute and relative tolerance values for the integration can be set by the user. The integration goes on until one of the following stop conditions is fulfilled (more details in Vincent *et al* (2011)):

- The plasma becomes optically thick,
- The photon escapes too far from the area of interest (could be set by the user),
- The photon approaches too closely to the event horizon,
- The number of integration steps reach the maximum.

Given that the parallel transport preserves the scalar product between vectors[10], and given that $(\mathbf{k}, \bar{\mathbf{w}}, \bar{\mathbf{n}})$ are mutually orthogonal at the observer, they remain mutually orthogonal when parallel-transported at the emitter, and $\bar{\mathbf{w}}$ and $\bar{\mathbf{n}}$ remain unit vectors.

It is useful at this point to note that, in vacuum, the EVPA is a conserved quantity along a geodesic. Let us demonstrate this result. We have seen that, at the distant observer's location, we might confuse the covariant and non-covariant polarization vectors, $\hat{\mathbf{f}}_0$ and $\hat{\mathbf{F}}_0$. Let us consider the point along a photon's geodesic corresponding to the exit from the emitting source region, meaning that the part of the geodesic located in between this point and the distant observer is in vacuum. We hereafter call this point the exit point. We can make the exact same reasoning at the exit point as we made at the distant observer's location, and conclude that we can confuse the covariant and non-covariant polarization vectors at the exit point, $\hat{\mathbf{f}}_{\text{exit}}$ and $\hat{\mathbf{F}}_{\text{exit}}$, where $\hat{\mathbf{F}}_{\text{exit}}$ is the polarization vector as measured by the emitter at the exit point. This implies more generally that $\hat{\mathbf{f}}$ and $\hat{\mathbf{F}}$ can be confused at any point along the part of the geodesic located in vacuum. Given that $\hat{\mathbf{f}}$ and the screen basis $(\bar{\mathbf{w}}, \bar{\mathbf{n}})$ are parallel propagated along the geodesic in vacuum (see equations (8) and (31)), the angle between $\hat{\mathbf{f}}$ and the basis vectors is conserved in vacuum, hence the EVPA is conserved along the part of the geodesic located in vacuum. This is of course no longer valid in the source region, where the covariant polarization vector is no longer parallel propagated (the parallel propagation of $\hat{\mathbf{f}}$ is a consequence of Maxwell's equations in vacuum).

---

[10] This is an obvious property: let us consider two vectors a^μ and b^μ parallel-transported along k^μ, then $\nabla_{\mathbf{k}}(\mathbf{a} \cdot \mathbf{b}) = k^\mu \nabla_\mu (g_{\alpha\beta} a^\alpha b^\beta) = g_{\alpha\beta} (a^\alpha k^\mu \nabla_\mu b^\beta + b^\beta k^\mu \nabla_\mu a^\alpha) = 0$, because of the parallel-transport relations $k^\mu \nabla_\mu a^\alpha = 0$ and $k^\mu \nabla_\mu b^\beta = 0$. We used the fact that the connexion ∇ is compatible with the metric to get $\nabla_\mu g_{\alpha\beta} = 0$ and take the metric tensor out of the covariant derivative.

We want to project the parallel-transported basis vectors $(\mathbf{k}, \bar{\mathbf{w}}, \bar{\mathbf{n}})$ orthogonally to the 4-velocity $\mathbf{u}$ of the emitting fluid, that is, project them in the local rest space of the fluid. By doing so without further precaution, we would of course lose the mutual orthogonality between these vectors, which is not preserved in a projection. Let us consider

$$
\begin{aligned}
\bar{\mathbf{w}}' &= \bar{\mathbf{w}} - \frac{\bar{\mathbf{w}} \cdot \mathbf{u}}{\mathbf{k} \cdot \mathbf{u}} \mathbf{k}, \\
\bar{\mathbf{n}}' &= \bar{\mathbf{n}} - \frac{\bar{\mathbf{n}} \cdot \mathbf{u}}{\mathbf{k} \cdot \mathbf{u}} \mathbf{k},
\end{aligned}
\tag{32}
$$

where the denominator, $\mathbf{k} \cdot \mathbf{u}$, is minus the energy of the photon as measured in the fluid frame, and as such, non zero, so that these expressions are well defined. It is easy to check that these two vectors are spacelike unit vectors, orthogonal to $\mathbf{u}$, to each other, and to

$$
\bar{\mathbf{K}} = \frac{\mathbf{k} + (\mathbf{k} \cdot \mathbf{u})\, \mathbf{u}}{|\mathbf{k} \cdot \mathbf{u}|},
\tag{33}
$$

the normalized projection of $\mathbf{k}$ orthogonal to $\mathbf{u}$, which coincides with the unit direction of emission of the photon in the fluid frame. We thus obtain a well-defined orthonormal direct triad $(\bar{\mathbf{K}}, \bar{\mathbf{w}}', \bar{\mathbf{n}}')$ of the fluid frame, illustrated in figure 3. We note that if we consider a vector $\mathbf{F}$ in the fluid frame, normal to $\bar{\mathbf{K}}$, then our definition leads to

$$
\mathbf{F} \cdot \bar{\mathbf{n}} = \mathbf{F} \cdot \bar{\mathbf{n}}',
\tag{34}
$$

and similarly for $\mathbf{w}$, so that our definition allows to keep unchanged the angles between such a vector $\mathbf{F}$ and the reference directions, be they primed or unprimed. This will be important later.

Let us now consider the magnetic field 4-vector $\mathbf{b}$ of the accretion flow, as measured in the fluid frame. By construction, this vector lies in the local rest frame of the fluid, so it is orthogonal to $\mathbf{u}$. We are also interested in its normalized projection orthogonally to $\bar{\mathbf{K}}$, which reads

$$
\bar{\boldsymbol{b}}_\perp = \frac{\mathbf{b} - (\mathbf{b} \cdot \bar{\mathbf{K}})\, \bar{\mathbf{K}}}{||\mathbf{b} - (\mathbf{b} \cdot \bar{\mathbf{K}})\, \bar{\mathbf{K}}||},
\tag{35}
$$

(note that the minus sign in the numerator and denominator of the rhs, compared to the plus sign in the numerator of the rhs of equation (33), comes from the fact that $\bar{\mathbf{K}}$ is spacelike while $\mathbf{u}$ is timelike), and in the unit polarization vector as measured in the fluid frame

$$
\bar{\mathbf{F}} = \frac{\bar{\mathbf{K}} \times \mathbf{b}}{||\bar{\mathbf{K}} \times \mathbf{b}||} = \bar{\mathbf{K}} \times \bar{\boldsymbol{b}}_\perp.
\tag{36}
$$

We thus have constructed a second orthonormal direct triad of the fluid rest space, $(\bar{\mathbf{K}}, \bar{\boldsymbol{b}}_\perp, \bar{\mathbf{F}})$. We note that it is not obvious that the vector defined by equation (36) coincides with the emission polarization vector for synchrotron radiation, that is, with the direction of the radiation electric field emitted by an electron moving around the $\mathbf{b}$ field lines, given that we have never discussed the emitting electron motion so far. In appendix B, by relating the particle frame and the fluid frame, we demonstrate that, provided the emitting electron is relativistic, this is indeed so.
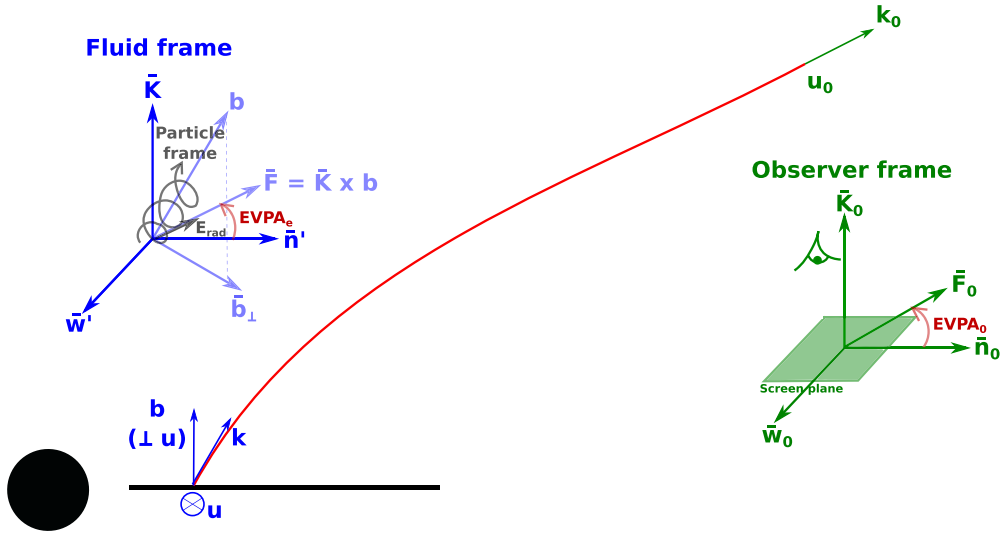
Figure 3. Frames of interest for the polarized ray-tracing problem. The far-away observer's rest frame (orthogonal to the observer's 4-velocity $\mathbf{u_0}$) is shown in green, it is a simplified version of figure 1 and shows the local incidence direction $\bar{\mathbf{K}}_0$ (spacelike vector) of the observed light ray, together with the null 4-vector tangent to the incident null geodesic $\mathbf{k_0}$, the local North and West spacelike directions $(\bar{\mathbf{w}}_0, \bar{\mathbf{n}}_0)$, such that $(\bar{\mathbf{K}}_0, \bar{\mathbf{w}}_0, \bar{\mathbf{n}}_0)$ is a direct orthonormal triad, and the polarization vector as measured by the far-away observer, $\bar{\mathbf{F}}_0$. The observed EVPA is labelled EVPA_0, lying between the screen's North direction and the observed polarization vector $\bar{\mathbf{F}}_0$. Starting from the far-away observer, a null geodesic is integrated backwards towards the source (red line), until it reaches the accretion flow (black line) surrounding the black hole (black disk). The fluid frame (orthogonal to the emitter's 4-velocity $\mathbf{u}$) is shown in blue. The null 4-vector tangent to the null geodesic at the emission point is called $\mathbf{k}$. The magnetic field spacelike 4-vector as measured in the fluid frame (thus, orthogonal to $\mathbf{u}$) is called $\mathbf{b}$. The synchrotron-emitting electron's trajectory is represented by the pale black helix. The local direction of photon emission, as measured in the fluid frame, is the spacelike unit vector $\bar{\mathbf{K}}$. The pair of vectors $(\bar{\mathbf{n}}', \bar{\mathbf{w}}')$ is related to the pair $(\bar{\mathbf{n}}_0, \bar{\mathbf{w}}_0)$, parallel-propagated along the null geodesic (see text for details), such that $(\bar{\mathbf{K}}, \bar{\mathbf{w}}', \bar{\mathbf{n}}')$ is a direct orthonormal triad. The unit polarization vector as measured by the emitter is called $\bar{\mathbf{F}}$. The radiation field $\mathbf{E}_{\text{rad}}$ associated with the helical motion of the electron is shown in pale black, and lies along $\bar{\mathbf{F}}$ for a relativistic electron (see appendix B for a demonstration). The unit projection of the magnetic 4-vector orthogonal to $\bar{\mathbf{K}}$ is called $\bar{\boldsymbol{b}}_\perp$. Thus $(\bar{\mathbf{K}}, \bar{\boldsymbol{b}}_\perp, \bar{\mathbf{F}})$ is also a direct orthonormal triad, rotated with respect to $(\bar{\mathbf{K}}, \bar{\mathbf{w}}', \bar{\mathbf{n}}')$ by the emission EVPA, labeled EVPA_e, lying between the parallel-transported North direction and the fluid-frame polarization vector $\bar{\mathbf{F}}$.

We have thus at hand two orthonormal triads of the fluid frame, the observer-related $(\bar{\mathbf{K}}, \bar{\mathbf{w}}', \bar{\mathbf{n}}')$, and the magnetic-field-related $(\bar{\mathbf{K}}, \bar{\boldsymbol{b}}_\perp, \bar{\mathbf{F}})$. These two frames are rotated with respect to each other by the angle

$$\chi \equiv \left(\bar{\mathbf{n}}', \bar{\mathbf{F}}\right) = \left(\bar{\mathbf{n}}, \bar{\mathbf{F}}\right) \equiv \text{EVPA}_e, \tag{37}$$

the EVPA in the fluid frame, where the index e reminds that we are dealing with an emission EVPA, as compared to the observed EVPA of figure 1. Both angles are illustrated in figure 3. We note that the emission EVPA evolves as the light ray evolves through the emitting fluid; the EVPA is only conserved in vacuum as demonstrated above. So a sequence of emission EVPAs
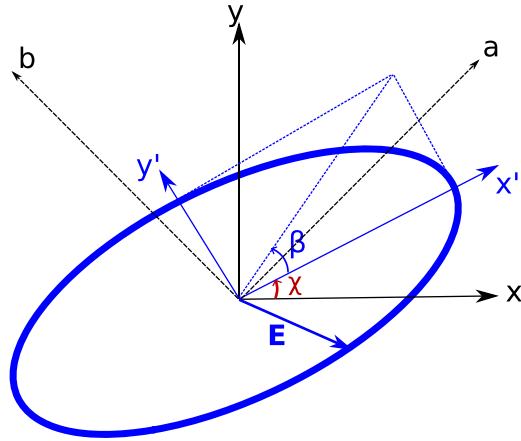
Figure 4. Polarization ellipse of a general monochromatic wave (in blue). The black axes (x, y) label the frame of interest where we want to formulate the problem, while the blue axes (x', y') are along the major and minor axes of the ellipse and are therefore naturally adapted to the elliptically polarized wave. The angle between the two bases is called χ (it would coincide with the notion of EVPA for a linearly polarized wave along the x axis), and the quantity $\tan \beta$ encodes the ellipse axes ratio. The dashed black axes (a, b) are tilted by $45°$ relative to (x, y) and are useful for defining the U Stokes parameter.

corresponds to a unique observed EVPA. Note that the second equality in equation (37) is a consequence of equation (34). This emission EVPA will be crucial in the polarized radiative transfer formalism that we introduce in the next section. A practical, code-friendly expression for the emission EVPA is the following

$$\text{EVPA}_{\text{e}} = \frac{\pi}{2} - \text{atan2}\left(\bar{\mathbf{b}}_{\perp} \cdot \bar{\mathbf{w}}', \bar{\mathbf{b}}_{\perp} \cdot \bar{\mathbf{n}}'\right). \tag{38}$$

After having discussed the parallel transport of the vectors of interest along the null geodesic, the last step of the polarized GRRT problem is to integrate the polarized radiative transfer within the accretion flow surrounding the compact object.

2.4. Polarized radiative transfer

2.4.1. Stokes parameters. The most general monochromatic electromagnetic wave has an elliptical polarization, in the sense that the electric field vector describing the wave draws an ellipse during its time evolution in the plane normal to the direction of propagation, see figure 4.

Let us introduce the electric field complex vector of the monochromatic wave

$$\hat{\mathbf{E}} = \hat{E}_x \bar{\mathbf{e}}_x + \hat{E}_y \bar{\mathbf{e}}_y, \tag{39}$$

decomposed in an arbitrary orthonormal basis $(\bar{\mathbf{e}}_x, \bar{\mathbf{e}}_y)$ of the plane orthogonal to the direction of propagation, where $\hat{E}_x$ and $\hat{E}_y$ are the complex components along the axes. The polarization ellipse described by the vector $\hat{\mathbf{E}}$ can be equivalently described by two sets of parameters. From a geometrical point of view, it is very natural to provide the total intensity $|\hat{\mathbf{E}}|^2$, together with two angles χ and β. The angle χ lies between the basis $(\bar{\mathbf{e}}_x, \bar{\mathbf{e}}_y)$ and the basis corresponding

to the axes of the ellipse, while $\tan\beta$ encodes the ellipse axes ratio (see figure 4). However, this parametrization is not practical from a physical point of view given that the two angles are not directly observable. So from a physical point of view, it is more natural to consider the following set of four Stokes parameters (Rybicki and Lightman 1979)

$$
\begin{aligned}
I &= |\hat{E}_x|^2 + |\hat{E}_y|^2, \\
Q &= |\hat{E}_x|^2 - |\hat{E}_y|^2 = I\cos 2\chi \,\cos 2\beta, \\
U &= |\hat{E}_a|^2 - |\hat{E}_b|^2 = I\sin 2\chi \,\cos 2\beta, \\
V &= |\hat{E}_r|^2 - |\hat{E}_l|^2 = I\sin 2\beta,
\end{aligned}
\tag{40}
$$

where $\hat{E}_a$ and $\hat{E}_b$ are the complex components of the electric field in an orthonormal basis $(\bar{\mathbf{e}}_a, \bar{\mathbf{e}}_b)$ rotated by $45°$ compared to $(\bar{\mathbf{e}}_x, \bar{\mathbf{e}}_y)$, see the dashed black axes in figure 4. The quantities $\hat{E}_r$ and $\hat{E}_l$ are the complex components of the field in an orthonormal complex basis, $\bar{\mathbf{e}}_{l,r} = \sqrt{2}/2(\bar{\mathbf{e}}_x \pm i\,\bar{\mathbf{e}}_y)$. These relations clearly show that the Stokes parameters are all sums or differences of intensities along specific directions, and as such are directly observable and well adapted to being evolved in a radiative transfer problem. Equation (40) show how to construct the Stokes parameters from the geometrical angular parameters χ, β of the polarization ellipse. The reverse expression is easy to find and reads

$$
\begin{aligned}
\tan 2\chi &= \frac{U}{Q}, \\
\sin 2\beta &= \frac{V}{I}.
\end{aligned}
\tag{41}
$$

For a circular polarization, $\beta = \pi/4$, so

$$
Q = 0, \quad U = 0, \quad V = I \quad \text{(circular polarization)},
\tag{42}
$$

while for a linear polarization, $\beta = 0$, and

$$
Q = I\cos 2\chi, \quad U = I\sin 2\chi, \quad V = 0 \quad \text{(linear polarization)},
\tag{43}
$$

and if the wave is polarized along the x axis of figure 4, then $Q = I$ and $U = 0$, while if the wave is polarized at $45°$ from the x axis, then $Q = 0$ and $U = I$. So Q and U encode linear polarization along the directions $\bar{\mathbf{e}}_x$ or $\bar{\mathbf{e}}_y$ and $\bar{\mathbf{e}}_a$ or $\bar{\mathbf{e}}_b$, respectively, and V encodes circular polarization.

Let us consider the Stokes parameters (I, Q, U, V) defined in a basis $(\bar{\mathbf{e}}_x, \bar{\mathbf{e}}_y)$, and the parameters (I', Q', U', V') defined in a basis $(\mathbf{e}'_x, \mathbf{e}'_y)$, rotated by an angle χ with respect to $(\bar{\mathbf{e}}_x, \bar{\mathbf{e}}_y)$, see figure 4. It is easy to show that the Q and U Stokes parameters transform following

$$
\begin{pmatrix} Q \\ U \end{pmatrix} = \begin{pmatrix} \cos 2\chi & -\sin 2\chi \\ \sin 2\chi & \cos 2\chi \end{pmatrix} \begin{pmatrix} Q' \\ U' \end{pmatrix},
\tag{44}
$$

while I and V are invariant.

For a monochromatic radiation, there must exist a relation between the four Stokes parameters, that are equivalent to the set of three parameters (I, χ, β), and thus cannot be independent. This relation reads

$$
I^2 = Q^2 + U^2 + V^2 \quad \text{(monochromatic / fully polarized)}
\tag{45}
$$

and the radiation is then said to be fully polarized. For a superimposition of waves at different frequencies, the radiation is only partially polarized and the resulting Stokes parameters verify

$$I^2 \geqslant Q^2 + U^2 + V^2 \quad \text{(partially polarized)} . \tag{46}$$

It is then useful to introduce the degree of polarization

$$d_p = \frac{\sqrt{Q^2 + U^2 + V^2}}{I}, \tag{47}$$

and the degree of linear polarization

$$d_{lp} = \frac{\sqrt{Q^2 + U^2}}{I}. \tag{48}$$

2.4.2. Stokes parameters for synchrotron radiation, conventions.　　We are primarily interested in polarized synchrotron radiation given that our main science interest is the millimeter and infrared radiation emitted by nearby supermassive black hole environments. Let us consider a single electron following a helical motion around the field lines of a magnetic field **b** as measured in the fluid frame. The emitted synchrotron radiation is elliptically polarized, with the minor axis of the polarization ellipse aligned along the direction of the magnetic field projected orthogonally to the direction of propagation, and major axis along the fluid-frame polarization vector (Huang *et al* 2009). The Stokes parameters are thus naturally expressed in a basis aligned with the axes of this polarization ellipse, that is, the $(\bar{\mathbf{F}}, -\bar{\mathbf{b}}_\perp)$ basis (see the illustration in figure 5). We call this basis the *synchrotron polarization basis*. This basis is rotated by the emission EVPA with respect to the observer-related $(\bar{\mathbf{n}}', -\bar{\mathbf{w}}')$ basis. This last basis is called the *parallel-transported polarization basis*. For integrating the radiative transfer in the observer's frame, we will need to take care of this rotation between the synchrotron and the parallel-transported polarization bases. This is described in the next section.

Our sign conventions for the Stokes parameters are illustrated in figure 5. It complies with the convention of the International Astronomical Union (Transactions of the International Astronomical Union 1973, Hamaker and Bregman 1996, see figure 1 of the second reference).

2.4.3. Transfer equation.　　Just like in the unpolarized version of Gyoto (Vincent *et al* 2011), we will integrate the radiative transfer equation in the fluid frame, and then transform the quantities to the observer's frame. The unpolarized radiative transfer equation used by Gyoto reads

$$\frac{dI_\nu^{em}}{ds} = j_\nu - \alpha_\nu I_\nu^{em}, \tag{49}$$

where I_ν^{em} is the specific intensity (the index ν means that we are considering an intensity per unit of frequency), ds is the element of optical path length, j_ν and α_ν are the specific emission and absorption coefficients, all these quantities being measured in the fluid frame (hence the superscript 'em' for the intensity, referring to the emitting fluid; we discard it for the other quantities for simplicity). The intensity in the observer frame (superscript 'obs') then follows from

$$I_\nu^{obs} = I_\nu^{em} \left(\frac{\nu^{obs}}{\nu^{em}} \right)^3, \tag{50}$$
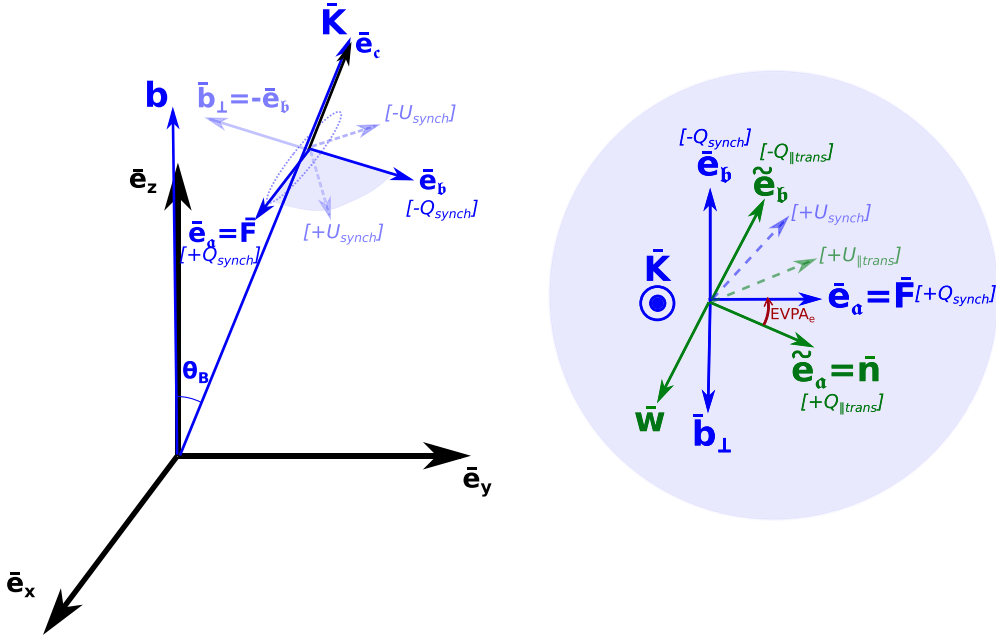
Figure 5. Geometry of the polarized synchrotron problem and Stokes parameter illustration. All quantities depicted here are defined in the fluid frame. The magnetic field is **b**, which lies along the $\bar{\mathbf{e}}_z$ unit vector. The direction of emission in this frame is $\bar{\mathbf{K}}$, which lies along the $\bar{\mathbf{e}}_c$ unit vector. We define the $\bar{\mathbf{e}}_a$ unit vector as lying along the major axis of the synchrotron polarization ellipse (shown in dashed pale blue). This vector is defined up to an unimportant sign convention. The $\bar{\mathbf{e}}_b$ unit vector is such that $(\bar{\mathbf{e}}_a, \bar{\mathbf{e}}_b, \bar{\mathbf{e}}_c)$ is a direct orthonormal triad of the fluid frame. The vector $\bar{\mathbf{e}}_x$ is parallel to $\bar{\mathbf{e}}_a$. The $\bar{\mathbf{e}}_y$ unit vector is such that $(\bar{\mathbf{e}}_x, \bar{\mathbf{e}}_y, \bar{\mathbf{e}}_z)$ is a direct orthonormal triad of the fluid frame. The angle between **b** and $\bar{\mathbf{K}}$ is called θ_B. The Stokes parameters Q and U are defined in the $(\bar{\mathbf{e}}_a = \mathbf{F}, \bar{\mathbf{e}}_b = -\bar{\mathbf{b}}_\perp)$ basis, that we call the synchrotron polarization basis, illustrated by the zoom on the right of the figure. This zoom shows the synchrotron polarization basis (in blue; subscript 'synch') as well as the parallel-transported polarization basis (in green; subscript '∥trans'), $(\mathbf{e}_a = \bar{\mathbf{n}}, \mathbf{e}_b = -\bar{\mathbf{w}})$. These two bases are rotated by the emission EVPA angle. The sign conventions of the Stokes parameters are as shown in this zoom. Note that the orientation convention used in this figure is the same as that used by e.g. Huang and Shcherbakov (2011), Dexter (2016), which results in a positive emission coefficient for Stokes Q. Some authors use an alternative orientation convention, taking $\bar{\mathbf{e}}_a$ along the minor axis of the polarization ellipse, see Shcherbakov (2008), Marszewski *et al* (2021). This simply leads to Stokes Q being multiplied by -1, and to a negative emission coefficient for Stokes Q.

which is a consequence of Liouville's theorem (Misner *et al* 1973).

The polarized radiative transfer equation is naturally written in the synchrotron polarization basis of the fluid frame. In this basis, the transfer equation reads

$$\frac{\mathrm{d}}{\mathrm{d}s}\begin{pmatrix} I_\nu^{\mathrm{em;synch}} \\ Q_\nu^{\mathrm{em;synch}} \\ U_\nu^{\mathrm{em;synch}} \\ V_\nu^{\mathrm{em;synch}} \end{pmatrix} = \begin{pmatrix} j_{\nu,I} \\ j_{\nu,Q} \\ j_{\nu,U} \\ j_{\nu,V} \end{pmatrix} - \begin{pmatrix} \alpha_{\nu,I} & \alpha_{\nu,Q} & \alpha_{\nu,U} & \alpha_{\nu,V} \\ \alpha_{\nu,Q} & \alpha_{\nu,I} & r_{\nu,V} & -r_{\nu,U} \\ \alpha_{\nu,U} & -r_{\nu,V} & \alpha_{\nu,I} & r_{\nu,Q} \\ \alpha_{\nu,V} & r_{\nu,U} & -r_{\nu,Q} & \alpha_{\nu,I} \end{pmatrix} \begin{pmatrix} I_\nu^{\mathrm{em;synch}} \\ Q_\nu^{\mathrm{em;synch}} \\ U_\nu^{\mathrm{em;synch}} \\ V_\nu^{\mathrm{em;synch}} \end{pmatrix},$$

$$(51)$$

where the 'em;synch' label is here to remind that we are dealing with Stokes parameters expressed in the synchrotron polarization basis of the emitting fluid frame; moreover, $j_{\nu,X}$ and $\alpha_{\nu,X}$ are emission and absorption coefficients for the Stokes parameter X, $r_{\nu,Q}$ and $r_{\nu,U}$ are Faraday conversion parameters, and $r_{\nu,V}$ is the Faraday rotation parameter. All these transfer coefficients are defined in the synchrotron polarization basis of the fluid frame (we discard the superscript for simplicity). We refer to figure 5 for the details of the sign conventions.

However, we rather want to integrate this equation in the parallel-transported polarization basis, $(\bar{\mathbf{n}}', -\bar{\mathbf{w}}')$, which is rotated by the emission EVPA with respect to the synchrotron polarization basis, see figure 5. In the parallel-transported polarization basis of the fluid frame, the transfer equation reads

$$
\frac{\mathrm{d}}{\mathrm{d}s}
\begin{pmatrix}
I_\nu^{\mathrm{em};\|\mathrm{trans}} \\
Q_\nu^{\mathrm{em};\|\mathrm{trans}} \\
U_\nu^{\mathrm{em};\|\mathrm{trans}} \\
V_\nu^{\mathrm{em};\|\mathrm{trans}}
\end{pmatrix}
= \mathbf{R}(\chi_{\mathrm{e}})
\begin{pmatrix}
j_{\nu,I} \\
j_{\nu,Q} \\
j_{\nu,U} \\
j_{\nu,V}
\end{pmatrix}
$$

$$
- \mathbf{R}(\chi_{\mathrm{e}})
\begin{pmatrix}
\alpha_{\nu,I} & \alpha_{\nu,Q} & \alpha_{\nu,U} & \alpha_{\nu,V} \\
\alpha_{\nu,Q} & \alpha_{\nu,I} & r_{\nu,V} & -r_{\nu,U} \\
\alpha_{\nu,U} & -r_{\nu,V} & \alpha_{\nu,I} & r_{\nu,Q} \\
\alpha_{\nu,V} & r_{\nu,U} & -r_{\nu,Q} & \alpha_{\nu,I}
\end{pmatrix}
\mathbf{R}(-\chi_{\mathrm{e}})
\begin{pmatrix}
I_\nu^{\mathrm{em};\|\mathrm{trans}} \\
Q_\nu^{\mathrm{em};\|\mathrm{trans}} \\
U_\nu^{\mathrm{em};\|\mathrm{trans}} \\
V_\nu^{\mathrm{em};\|\mathrm{trans}}
\end{pmatrix},
\tag{52}
$$

where the superscript 'em;‖trans' reminds that we are dealing with Stokes parameters defined in the parallel-transported polarization basis of the emitting fluid frame, and

$$
\mathbf{R}(\chi_{\mathrm{e}}) =
\begin{pmatrix}
1 & 0 & 0 & 0 \\
0 & \cos 2\chi_{\mathrm{e}} & -\sin 2\chi_{\mathrm{e}} & 0 \\
0 & \sin 2\chi_{\mathrm{e}} & \cos 2\chi_{\mathrm{e}} & 0 \\
0 & 0 & 0 & 1
\end{pmatrix}
\tag{53}
$$

is a rotation matrix describing the rotation by the angle $\chi_{\mathrm{e}} \equiv \mathrm{EVPA}_{\mathrm{e}}$, the emission EVPA, between the synchrotron and the parallel-transported polarization bases. This is the exact same transformation as that described by equation (44).

Solving equation (52) is a well-known problem that we briefly discuss in appendix C. The corresponding Stokes parameters in the observer frame then follow from

$$
X_\nu^{\mathrm{obs}} = X_\nu^{\mathrm{em};\|\mathrm{trans}} \left(\frac{\nu^{\mathrm{obs}}}{\nu^{\mathrm{em}}} \right)^3,
\tag{54}
$$

similarly as in equation (50), where X is either of the Stokes parameters.

2.4.4. Polarized synchrotron coefficients. We now need to express the synchrotron coefficients in the synchrotron polarization basis. In this basis, the transfer coefficients for the Stokes parameter U, i.e. $j_{\nu,U}$, $\alpha_{\nu,U}$ and $r_{\nu,U}$ are zero by definition. However, the computation of emission, absorption and rotation synchrotron coefficients for the others Stokes parameters, from an arbitrary distribution of electrons could be quite heavy. Indeed, even for isotropic distributions, the computation of the emission coefficients require a double integral (Rybicki and

Lightman 1979) and the others are even more complex using the susceptibility tensor (see appendix B of Marszewski *et al* 2021). Fortunately, Huang and Shcherbakov (2011), Dexter (2016), Marszewski *et al* (2021) derived fitted formulae for the emissivities, absorptivities and rotativities for well-defined isotropic distributions of electrons : Thermal (Maxwell-Jüttner), Power Law or Kappa (thermal core with a power law tail). We choose to implement the formulae of Marszewski *et al* (2021) in GYOTO to compute the synchrotron coefficients as they are the only one who provides formulae for a kappa distribution. These formulae are valid for a specific range of parameters.

For a thermal distribution, parametrized by the dimensionless temperature $\Theta_e = k_B T/m_e c^2$, the fits are accurate for $3 < \Theta_e < 40$ and for $\nu/\nu_c \gg 1$ with $\nu_c = eB/(2\pi m_e c)$ the cyclotron frequencies (Marszewski *et al* 2021).

For a Power Law distribution, parametrized by a minimum and maximum Lorentz factor, $\gamma_{\min}$ and $\gamma_{\max}$ respectively, and by a power law index p, the fits are accurate for $\gamma_{\min} < 10^2$, $1.5 < p < 6.5$ and, as before, for $\nu/\nu_c \gg 1$ (Marszewski *et al* 2021).

The Kappa distribution is characterized by two parameters w (equivalent to the dimensionless temperature) and $\kappa = p + 1$. Contrary to the other distributions where the fits are continuous functions of the parameters, the fits for rotation coefficients for the Kappa distribution have been done for four specific values of $\kappa = (3.5, 4.0, 4.5, 5.0)$ and are not defined for any other value. The fits are valid while $3 < w < 40$, $\nu/\nu_c \gg 1$ and $X_\kappa \gg 10^{-1}$ where $X_\kappa = \nu/\nu_c (w\kappa)^2 \sin\theta$ with θ the angle between the magnetic field vector and the photon tangent vector (Marszewski *et al* 2021).

For some tests in section 3, we will use the formulae from Dexter (2016), especially for the comparison with the ray-tracing code IPOLE which use the formulae of Dexter (2016) (as the code GRTRANS). The order of the maximum relative error between all the fits in Marszewski *et al* (2021) and the true values is of 30%. For the typical parameters of the accretion flow of Sgr A*, the difference between the formulae of Marszewski *et al* (2021) and Dexter (2016) is lower or equal to 10%.

3. Tests

3.1. Test of the parallel transport

The first test that we have to make is to check that the observer polarization basis' vectors, i.e. $\bar{\mathbf{n}}$ and $\bar{\mathbf{w}}$, are well parallel transported along the null geodesics. The parallel transport equation given by equation (31) is fully general and agnostic about the particular spacetime considered. However, in the special case of the Kerr spacetime, it is well known that the special algebraic kind of the spacetime allows the existence of the Walker-Penrose constant (Walker and Penrose 1970), defined as follows. If $\mathbf{k}$ is the tangent vector to a null geodesic, and if $\mathbf{f}$ is a vector orthogonal to $\mathbf{k}$ and parallel-transported along $\mathbf{k}$, then the following complex quantity

$$K_1 - iK_2 = (r - ia\cos\theta) \left[\left(k^t f^r - k^r f^t\right) + a\sin^2\theta \left(k^r f^\varphi - k^\varphi f^r\right) \right.$$
$$\left. - i\sin\theta \left\{ \left(r^2 + a^2\right) \left(k^\varphi f^\theta - k^\theta f^\varphi\right) - a\left(k^t f^\theta - k^\theta f^t\right) \right\} \right], \qquad (55)$$

here expressed in Boyer–Lindquist coordinates, is conserved along the null geodesic. Thus, knowing the evolution of $\mathbf{k}$ along the null geodesic, the vectors $\bar{\mathbf{n}}$ and $\bar{\mathbf{w}}$ (that obviously fulfill

the conditions on **f** in equation (55)) can be immediately obtained without further computation by using this constant. This Kerr-specific result is only used for testing purposes in GYOTO. The code is agnostic about the spacetime and does not use this property.

We thus check the conservation of K_1 and K_2 for specific geodesics and obtain a conservation to within 10^{-5} for default integration parameters of GYOTO (relative and absolute tolerance value of 10^{-6}). This can be improved by setting a lower tolerance value for the integration steps, but at the cost of a longer calculation time.

3.2. EVPA calculation test

Parallel transport having been tested, the observer polarization basis is well defined in the rest frame of the emitter $(\bar{\mathbf{K}}, \bar{\mathbf{w}}', \bar{\mathbf{n}}')$, through equation (32). As said in section 2.3, the natural basis to express the synchrotron coefficients is $(\bar{\mathbf{K}}, \bar{\boldsymbol{b}}_\perp, \bar{\mathbf{F}})$ with $\bar{\mathbf{K}}$ a common vector between the two bases. Thus, to express the radiative transfer in the observer-related basis, rather than in the synchrotron basis, we just need to apply the rotation matrix defined in equation (53). The angle between these two bases corresponds to the emission EVPA (see section 2.3).

We define a simple setup to check the computation of this crucial angle. We consider a Page-Thorne disk (geometrically thin, optically thick; Page and Thorne 1974) in a Minkowski metric (to avoid GR effects), seen face-on. The screen resolution is 300×300 pixels with a field of view of $40\,r_g \mathrm{x} 40\,r_g$ and placed at a distance of $100\,r_g$. We consider two magnetic field configurations **b**, toroidal and radial. Expressed in Boyer–Lindquist coordinates, the two magnetic field configurations read, in the rest frame of the emitter

$$\textbf{Toroidal:}\ b^\alpha = \begin{cases} b^t = \sqrt{\frac{g_{\varphi\varphi}}{g_{tt}}\frac{\Omega^2}{g_{tt}+g_{\varphi\varphi}\Omega^2}}, \\ b^r = 0, \\ b^\theta = 0, \\ b^\varphi = \sqrt{\frac{g_{tt}}{g_{\varphi\varphi}}\frac{1}{g_{tt}+g_{\varphi\varphi}\Omega^2}}, \end{cases} \tag{56}$$

where $\Omega = u^\varphi/u^t$ and **u** is the 4-velocity of the emitting fluid assumed to be Keplerian, and

$$\textbf{Radial:}\ b^\alpha = \begin{cases} b^t = 0, \\ b^r = \sqrt{\frac{1}{g_{rr}}}, \\ b^\theta = 0, \\ b^\varphi = 0. \end{cases} \tag{57}$$

In the toroidal case, for all azimuthal angles of the disk, the wave-vector $\bar{\mathbf{K}}$ is made of two components, one almost vertical (face-on view), and one azimuthal component resulting from special-relativistic aberration (Vincent *et al* 2023). The magnetic field **b** is in the toroidal direction. Thus, the resulting polarization vector $\bar{\mathbf{F}} = \bar{\mathbf{K}} \times \bar{\boldsymbol{b}}_\perp$ is in the radial direction. Similarly, for the radial magnetic field, the resulting polarization vector is in the toroidal direction.

We consider an arbitrary $I_\nu = 1$ emission for unpolarized intensity. GYOTO computes images for the four Stokes parameters from which we can compute the orientation of the polarization vector, i.e. the EVPA. As we are only interested by the computation of the EVPA for the moment, i.e. without radiative transfer, we assume a fully linearly polarized radiation by taking $Q_\nu = I_\nu \cos(2*\mathrm{EVPA})$ and $U_\nu = I_\nu \sin(2*\mathrm{EVPA})$. This means that we do not take into account any absorption nor Faraday rotation.

We show in the left panel of figure 6 in background the unpolarized images of the setup described above and the polarization vector with the green ticks. The position angle of these
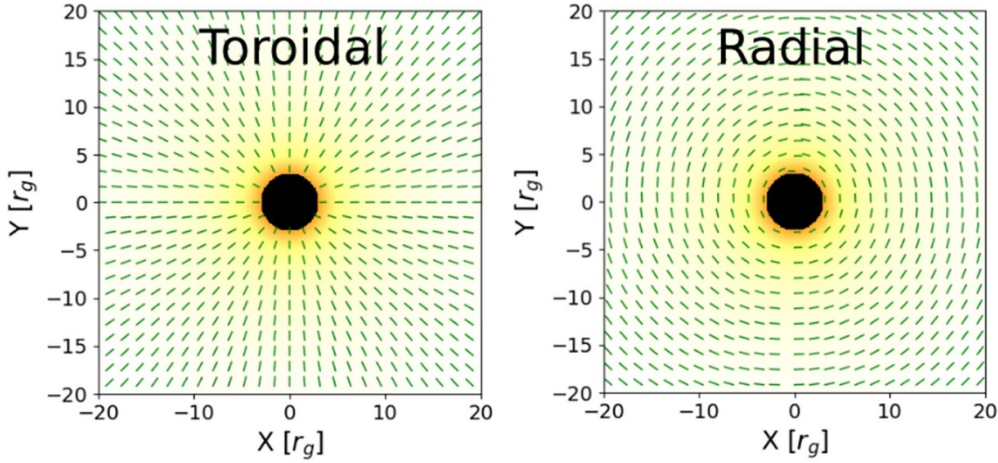
Figure 6. Image of total (unpolarized) intensity of a Page-Thorne disk with Keplerian orbit in a Minkowski space-time seen face-on for two magnetic field configurations (toroidal left, radial right). The inner radius is at $r = 3\,r_g$. The green lines represent the orientation of polarization vectors.

vectors is the observed EVPA. As expected, the polarization vectors are radial for a toroidal magnetic field and toroidal for radial magnetic field.

We now want to make a similar test in curved spacetime using a Kerr metric. To validate the computation of EVPA in GYOTO, we compute the polarization from a geometrically thin ring as in Gelles *et al* (2021) taking as previously $I_\nu = 1$, $Q_\nu = I_\nu \cos(2 * EVPA)$ and $U_\nu = I_\nu \sin(2 * EVPA)$. Gelles *et al* (2021) consider a synchrotron emission that we discard here, our only interest being in testing the EVPA. Here, we are only interested in the orientation of the polarization vector, that is, in the EVPA, at $r_1 = 3\,r_g$ and $r_2 = 6\,r_g$ (the inner and outer radius of the ring). Figure 7 shows the tick plots for three magnetic field configurations : radial, toroidal and vertical with the same setup as in figure 1 of Gelles *et al* (2021), the fluid being assumed to be comoving with the Zero Angular Momentum Observer frame. The vertical configuration implemented in GYOTO reads

$$
\textbf{Vertical } b^\alpha = \begin{cases} b^t = 0, \\ b^r = \frac{\cos\theta}{\sqrt{g_{rr}}}, \\ b^\theta = \frac{\sin\theta}{\sqrt{g_{\theta\theta}}}, \\ b^\varphi = 0. \end{cases} \tag{58}
$$

The results of GYOTO shown in figure 7 are in perfect agreement with the ones in the figure 1 in Gelles *et al* (2021). We note that Gelles *et al* (2021) scale the length of the ticks by the observed synchrotron intensity, while our ticks are all of unit length: we are only interested in the EVPA. This confirms that the calculation of the EVPA works correctly and we can now test the radiative transfer part and compare the results with another ray-tracing code.

3.3. Comparison with ipole

To check that all parts of our code work correctly, we compare the results of GYOTO with the ones of another polarized ray-tracing code : IPOLE (Mościbrodzka and Gammie 2018). We
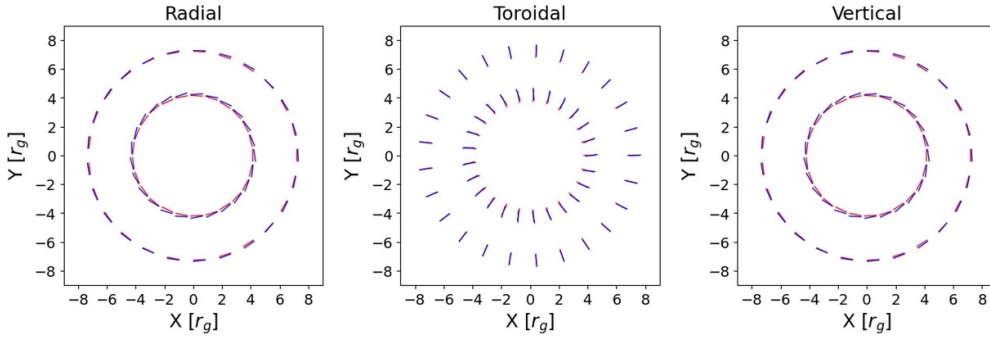
Figure 7. Polarized tick plots for three idealized magnetic field configurations: radial (left), toroidal (middle), and vertical (right) from a geometrically thin ring seen by an almost face-on observer $i = 0.1°$. The fluid is comoving with the zero angular momentum observer frame. Each plot shows two spins ($a = 0$ and $a = -0.99$ in red and blue, respectively) as two emission radii ($r_1 = 3\,r_g$ and $r_2 = 6\,r_g$, corresponding to the inner and outer rings, respectively).

will focus on polarized observables of a thick disk around a Schwarzschild black hole. We take power law profiles of the physical quantities following Vos *et al* (2022) (we invite the readers to refer to Vos *et al* (2022) for full details of the disk model). To compute the emission, absorption and rotation coefficients for the radiative transfer, we assume a thermal distribution of electrons (as in Vos *et al* 2022), and, for this comparison only, we use the fitting formula of Dexter (2016) as used in IPOLE (we remind that GYOTO implements the formulae from Marszewski *et al* 2021).

We compared the three magnetic field configurations (toroidal, radial and vertical) described in Vos *et al* (2022) at two inclinations, close to face-on with $i = 20°$ and close to edge-on with $i = 80°$. We define, as in Prather *et al* (2023), the normalized mean squared error (NMSE) as

$$\mathrm{NMSE}\,(A,B) = \frac{\sum |A_j - B_j|^2}{\sum |A_j|^2}, \tag{59}$$

where A_j and B_j are the intensities of a particular Stokes parameter in two images at pixel j. The results of GYOTO are in perfect agreement with IPOLE with a NMSE $<10^{-4}$ for all configurations and Stokes parameters except for Stoke U in the radial cases at high inclination for which the NMSE is around 10^{-3}. This can be compared to the worst NMSE of ~ 0.01 obtained in the code comparison made in Prather *et al* (2023) showing the perfect agreement between GYOTO and IPOLE.

We also performed pixel-to-pixel comparisons, not restricting our comparison to integrated quantities like the NMSE. Figure 8 illustrates this for 128×128 pixels images of the four Stokes parameters computed by GYOTO and their relative difference with IPOLE, in a field of view of $40\,r_g$, for the three magnetic field configurations described above, at low inclination $i = 20°$. The relative error map is very close to zero for the vast majority of pixels, with typical values $\lesssim 0.1\%$. Higher values are only reached on specific tracks, that correspond to the zeroes of the corresponding Stokes parameters (as is clear by comparing with the panels showing the maps of the corresponding Stokes parameters). It is thus not surprising to get higher residuals there, and it does not affect the radiative transfer, given that the Stokes parameters are anyway close to zero in these regions. Besides these tracks corresponding to the zeroes of the Stokes
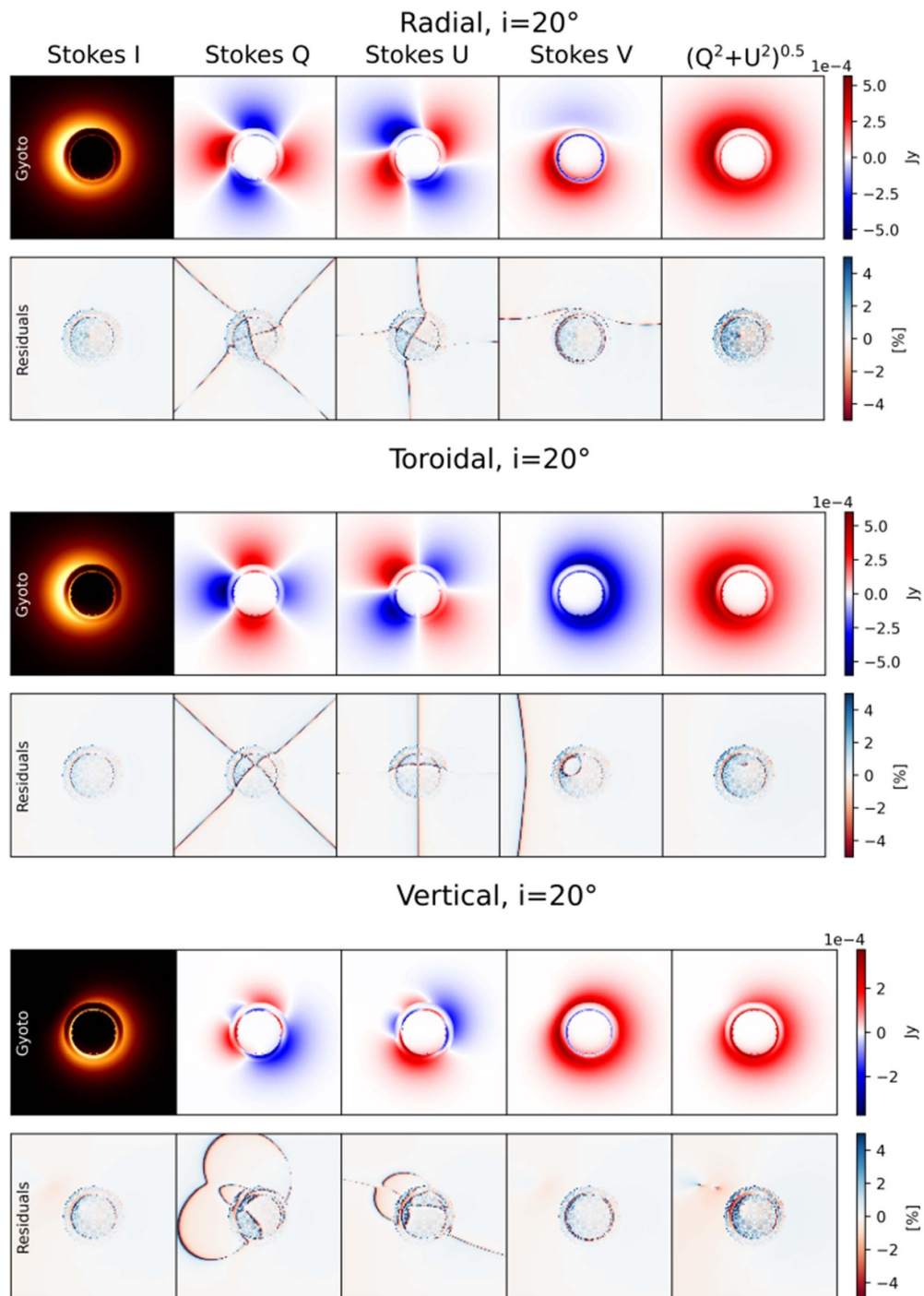
Figure 8. The first, third and fifth lines show images from left to right of the four Stokes parameters (I), (Q), (U), (V) generated by GYOTO and $Q^2 + U^2$ as the last column for the three magnetic field configuration at low inclination ($i = 20°$). Their relative error maps with IPOLE images are shown in the second, fourth and sixth lines. The relative errors scale is linear between $\pm 5\%$.

parameters, the interior of the 'shadow' region (i.e. geodesics that asymptotically approach the horizon when backward ray traced) lead to higher error. This is due to the stop condition of the geodesic integration that differs in the two codes. Given that this part of the image is anyway strongly redshifted and leads to a very low flux, this has no impact on the field-of-view integrated comparison of the NMSE.

4. Conclusion

This article presents the polarized version of the ray-tracing code GYOTO. After reviewing the formalism for polarized GRRT, our main aim is to explain the details of our implementation, and to provide tests of our code. In particular, we have shown that in the framework of the GRRT computation of a geometrically thick, optically thin accretion flow, we find results in perfect agreement with the IPOLE code.

Polarized GRRT is of fundamental importance for interpreting current and future observed data, in particular that of GRAVITY, the EHT, the polarized loops of ALMA associated with Sgr A* flares, or the data of IXPE. Properly interpreting these data is key to better understanding the properties of plasmas in the extreme environments of black holes, and might offer new interesting probes of strong-field gravity.

The polarized GYOTO code is public, actively maintained, and in constant development for offering ever more diversed setups for relativistic astrophysics. The recent polarized version of the code is accompanied by a python notebook, available at https://github.com/gyoto/Gyoto/blob/master/doc/examples/Gyoto_Polar_example.ipynb, offering a quick and user-friendly first example of the new environment.

Data availability statement

All data that support the findings of this study are included within the article (and any supplementary files).

Acknowledgments

Appendix A. Observer's screen polarization basis

A general vector $\bar{\mathbf{K}}_\mathbf{0}$, defined by the two spherical angles (a, b), see the right panel of figure 2, is obtained by rotating the vector $\bar{\mathbf{K}}_\mathbf{0}^{\mathrm{cen}}$ by an angle a in a plane containing $\bar{\mathbf{e}}_3$ and making an angle b with the $\bar{\mathbf{e}}_1$ vector (see the red plane in figure A1). This corresponds to a rotation of angle a around the vector $\mathbf{v} = -\sin b\,\bar{\mathbf{e}}_1 + \cos b\,\bar{\mathbf{e}}_2$. The corresponding rotation matrix reads
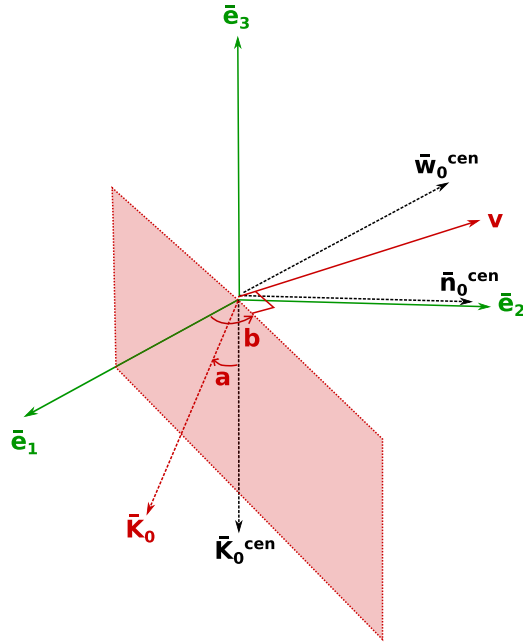
Figure A1. Local observer's basis $(\bar{\mathbf{e}}_1, \bar{\mathbf{e}}_2, \bar{\mathbf{e}}_3)$, in green, as represented in figure 2. The polarization basis corresponding to the central pixel of the screen, that is, to a purely radial direction of incidence, is $(\bar{\mathbf{K}}_0^{\mathrm{cen}}, \bar{\mathbf{w}}_0^{\mathrm{cen}}, \bar{\mathbf{n}}_0^{\mathrm{cen}})$, and is aligned with the oberver's local basis vectors. When considering a non-central pixel, the direction of photon incidence is no longer purely radial. The corresponding vector $\bar{\mathbf{K}}_0$ is obtained from $\bar{\mathbf{K}}_0^{\mathrm{cen}}$ by a rotation of angle a around the vector $\mathbf{v}$ (in red) normal to the red plane that contains $\bar{\mathbf{e}}_3$ and makes an angle b with $\bar{\mathbf{e}}_1$. The same applies for $\bar{\mathbf{w}}_0$ and $\bar{\mathbf{n}}_0$.

$$R(a,b) = \begin{pmatrix} \sin^2 b\,(1-\cos a) + \cos a & -\sin b \cos b\,(1-\cos a) & \cos b \sin a \\ -\sin b \cos b\,(1-\cos a) & \cos^2 b\,(1-\cos a) + \cos a & \sin b \cos a \\ -\cos b \sin a & -\sin b \sin a & \cos a \end{pmatrix}. \quad \text{(A.1)}$$

The general vector $\bar{\mathbf{K}}_0$ then reads $\bar{\mathbf{K}}_0 = R(a,b)\,\bar{\mathbf{K}}_0^{\mathrm{cen}}$, and similarly for the two other polarization vectors. It is then easy to express the general local unit West and North directions that complete the local incoming photon direction given by equation (27). They read

$$\bar{\mathbf{w}}_0 = \left[-\sin^2 b\,(1-\cos a) - \cos a\right]\bar{\mathbf{e}}_1 + \sin b \cos b\,(1-\cos a)\,\bar{\mathbf{e}}_2 + \cos b \sin a\,\bar{\mathbf{e}}_3,$$
$$\bar{\mathbf{n}}_0 = -\sin b \cos b\,(1-\cos a)\,\bar{\mathbf{e}}_1 + \left[\cos^2 b\,(1-\cos a) + \cos a\right]\bar{\mathbf{e}}_2 - \sin b \sin a\,\bar{\mathbf{e}}_3.$$
$$\text{(A.2)}$$

Appendix B. Electron gyration and polarization vector direction

Our discussion of the polarization vector in section 2.3 took place in the fluid frame. Here, we need to discuss a third natural frame (after the observer frame and the fluid frame) naturally associated with the GRRT problem, namely the particle frame, the frame comoving with an individual electron swirling around the magnetic field lines and emitting synchrotron
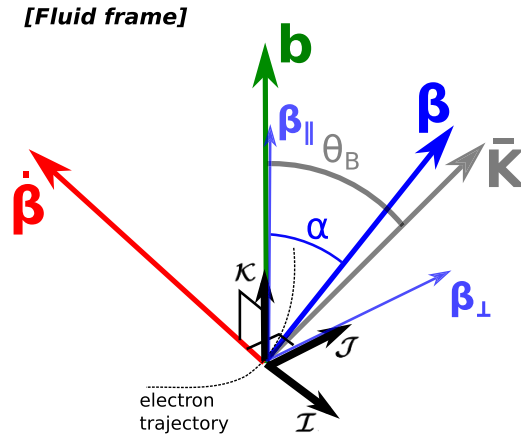
Figure B1. Geometry of the synchrotron-emitting electron motion in the fluid frame. $\boldsymbol{\beta}$ is the velocity 3-vector, $\bar{\mathbf{K}}$ is the direction of emission, $\mathbf{b}$ is the magnetic vector, all these quantities defined in the fluid frame. The emission angle between the magnetic field direction and the direction of emission is called θ_B while α is the pitch angle between the magnetic field direction and the velocity of the electron.

radiation as a consequence of this accelerated motion (see figure 3). The description of this infinitesimal[11] motion is the topic of this appendix. Our goal is to express the radiation electric field of an individual electron, as measured in the fluid frame. The direction of this vector should coincide with that of the polarization vector, which was introduced in equation (36) without any reference to the electron's motion, nor to its radiation field.

Let us consider the standard picture of synchrotron emission by a relativistic electron illustrated in figure B1, using the same notation and following the derivation of Westfold (1959). In the fluid frame, we consider a direct orthonormal triad, $(\mathcal{I}, \mathcal{J}, \mathcal{K})$, such that $\mathcal{I}$ is antiparallel to the acceleration vector at some initial time $t = 0$ (coinciding with the proper time of the fluid frame), $\mathcal{K}$ is along the ambient magnetic field $\mathbf{b}$ (measured in the fluid frame), and $\mathcal{J}$ completes the triad. We call $\boldsymbol{\beta}$ the velocity 3-vector of the electron in the fluid frame and $\dot{\boldsymbol{\beta}}$ the corresponding acceleration. A synchrotron wave is emitted by the accelerated electron in the unit direction $\bar{\mathbf{K}}$ (measured in the fluid frame). The emission angle θ_B and the pitch angle α are illustrated in figure B1.

The velocity and acceleration read

$$\boldsymbol{\beta} = \beta \sin\alpha \left(-\sin\omega_B t \, \mathcal{I} + \cos\omega_B t \, \mathcal{J}\right) + \beta \cos\alpha$$
$$\dot{\boldsymbol{\beta}} = -\omega_B \beta \sin\alpha \left(\cos\omega_B t \, \mathcal{I} + \sin\omega_B t \, \mathcal{J}\right), \mathcal{K}, \tag{B.1}$$

where β is the velocity of the electron in units of the speed of light, and ω_B is the cyclotron gyrofrequency. It is easy to check that at $t = 0$, the projection of the velocity vector orthogonal to $\mathbf{b}$ is along $\mathcal{J}$, and the acceleration vector is along $-\mathcal{I}$, which is the setup illustrated in figure B1.

The radiation field of the moving charge in the fluid frame satisfies

$$\mathbf{E}_{\text{rad}} \propto \bar{\mathbf{K}} \times \left[\left(\bar{\mathbf{K}} - \boldsymbol{\beta}\right) \times \dot{\boldsymbol{\beta}}\right]. \tag{B.2}$$

---

[11] Infinitesimal as compared to the natural scale of our problem coinciding with the gravitational radius.

Let us consider the unit direction of emission of a synchrotron photon, written in full generality as

$$\bar{\mathbf{K}} = a\mathcal{I} + b\mathcal{J} + c\mathcal{K}, \tag{B.3}$$

where (a,b,c) are arbitrary real numbers such that $\bar{\mathbf{K}}$ is a unit vector. It is easy to show that

$$\mathbf{E}_{\text{rad}} \cdot \mathcal{K} \propto \beta \cos\alpha - c. \tag{B.4}$$

The lhs quantity represents the projection of the radiating electric field along the ambient magnetic field direction. It is well known that the beaming effect leads to the radiation being confined within a narrow cone around the pitch angle of the relativistically moving electron (see figure 6.5 of Rybicki and Lightman 1979). This exactly means that

$$\beta \cos\alpha - c \approx 0, \tag{B.5}$$

such that the radiating electric field is orthogonal to the ambient magnetic field. It follows that

$$\mathbf{E}_{\text{rad}} \propto \bar{\mathbf{K}} \times \mathbf{b}, \tag{B.6}$$

so that the rhs can be used to define the direction of the synchrotron polarization vector, as done in equation (36).

Appendix C. Solving the polarized radiative transfer equation

Let us start with the unpolarized radiative transfer equation in the emitter frame

$$\frac{\mathrm{d}I}{\mathrm{d}s} = -\alpha I + j \tag{C.1}$$

with obvious notations. The formal solution reads

$$I(\tau) = \int_{s_0}^{s} \exp\left(-(\tau - \tau')\right) S(\tau') \, \mathrm{d}\tau' \tag{C.2}$$

where $S = j/\alpha$ is the source function, $\mathrm{d}\tau = \alpha \, \delta s$ is the optical depth, s is the proper length in the emitter frame and s_0 is some initial value of s where the intensity is assumed to be zero. This equation can equivalently be written

$$I(s) = \int_{s_0}^{s} \exp\left(-\alpha(s - s')\right) j(s') \, \mathrm{d}s', \tag{C.3}$$

where α is assumed constant over the integration interval. Considering a small range $\delta s = s - s'$ between some previous location s' and some current location s, over which interval j and α can be considered constant in a realistic problem, the increment of intensity reads

$$\delta I(s) = j(s) \, \delta s \exp\left(-\alpha(s) \, \delta s\right). \tag{C.4}$$

Let us now come back to the polarized version of the radiative transfer equation (equation (52)) which reads

$$\frac{\mathrm{d}\mathcal{I}}{\mathrm{d}s} = -\mathcal{K}\mathcal{I} + \mathcal{J}, \tag{C.5}$$

where $\mathcal{I}$ is the vector of Stokes parameters and

$$\mathcal{K} = \mathbf{R}(\chi) \begin{pmatrix} \alpha_I & \alpha_Q & \alpha_U & \alpha_V \\ \alpha_Q & \alpha_I & r_V & -r_U \\ \alpha_U & -r_V & \alpha_I & r_Q \\ \alpha_V & r_U & -r_Q & \alpha_I \end{pmatrix} \mathbf{R}(-\chi); \qquad \mathcal{J} = \mathbf{R}(\chi) \begin{pmatrix} j_I \\ j_Q \\ j_U \\ j_V \end{pmatrix} \tag{C.6}$$

with $\mathbf{R}(\chi)$ being the rotation matrix given in equation (53). Its formal solution is the direct generalization of equation (C.2), provided that $\mathcal{K}$ is constant with s:

$$\mathcal{I}(s) = \int_{s_0}^{s} \exp(-\mathcal{K}(s-s')) \mathcal{J}(s') \, \mathrm{d}s'. \tag{C.7}$$

Let us introduce the matrix

$$\mathbf{O}(s,s') = \exp(-\mathcal{K}(s-s')). \tag{C.8}$$

Over a small interval of proper length $\delta s = s - s'$, over which the absorption matrix and emission vector can be considered constant, the elementary increase of Stokes parameters is

$$\delta \mathcal{I}(s) = \mathbf{O}(\delta s) \mathcal{J}(s) \delta s \tag{C.9}$$

which is the direct generalization of equation (C.4). This is the equation used in GYOTO to update the Stokes parameters along the light ray.

We still need to compute the exponential of matrix appearing in equation (C.8). Landi Degl'Innocenti and Landi Degl'Innocenti (1985) have given an expression for this matrix. It reads

$$\begin{aligned} \mathbf{O}(\delta s) = \exp(-\alpha_I \delta s) \{ & [\cosh(\Lambda_1 \delta s) + \cos(\Lambda_2 \delta s)] \mathbf{M}_1/2 \\ & -\sin(\Lambda_2 \delta s) \mathbf{M}_2 \\ & -\sinh(\Lambda_1 \delta s) \mathbf{M}_3 \\ & + [\cosh(\Lambda_1 \delta s) - \cos(\Lambda_2 \delta s)] \mathbf{M}_4/2 \} \end{aligned} \tag{C.10}$$

with

$$\mathbf{M}_1 = 1,$$

$$\mathbf{M}_2 = \frac{1}{\Theta} \begin{pmatrix} 0 & \Lambda_2 \tilde{\alpha}_Q - \sigma \Lambda_1 \tilde{r}_Q & \Lambda_2 \tilde{\alpha}_U - \sigma \Lambda_1 \tilde{r}_U & \Lambda_2 \tilde{\alpha}_V - \sigma \Lambda_1 \tilde{r}_V \\ \Lambda_2 \tilde{\alpha}_Q - \sigma \Lambda_1 \tilde{r}_Q & 0 & \sigma \Lambda_1 \tilde{\alpha}_V + \Lambda_2 \tilde{r}_V & -\sigma \Lambda_1 \tilde{\alpha}_U - \Lambda_2 \tilde{r}_U \\ \Lambda_2 \tilde{\alpha}_U - \sigma \Lambda_1 \tilde{r}_U & -\sigma \Lambda_1 \tilde{\alpha}_V - \Lambda_2 \tilde{r}_V & 0 & \sigma \Lambda_1 \tilde{\alpha}_Q + \Lambda_2 \tilde{r}_Q \\ \Lambda_2 \tilde{\alpha}_V - \sigma \Lambda_1 \tilde{r}_V & \sigma \Lambda_1 \tilde{\alpha}_U + \Lambda_2 \tilde{r}_U & -\sigma \Lambda_1 \tilde{\alpha}_Q - \Lambda_2 \tilde{r}_Q & 0 \end{pmatrix},$$

$$\mathbf{M}_3 = \frac{1}{\Theta} \begin{pmatrix} 0 & \Lambda_1 \tilde{\alpha}_Q + \sigma \Lambda_2 \tilde{r}_Q & \Lambda_1 \tilde{\alpha}_U + \sigma \Lambda_2 \tilde{r}_U & \Lambda_1 \tilde{\alpha}_V + \sigma \Lambda_2 \tilde{r}_V \\ \Lambda_1 \tilde{\alpha}_Q + \sigma \Lambda_2 \tilde{r}_Q & 0 & -\sigma \Lambda_2 \tilde{\alpha}_V + \Lambda_1 \tilde{r}_V & \sigma \Lambda_2 \tilde{\alpha}_U - \Lambda_1 \tilde{r}_U \\ \Lambda_1 \tilde{\alpha}_U + \sigma \Lambda_2 \tilde{r}_U & \sigma \Lambda_2 \tilde{\alpha}_V - \Lambda_1 \tilde{r}_V & 0 & -\sigma \Lambda_2 \tilde{\alpha}_Q + \Lambda_1 \tilde{r}_Q \\ \Lambda_1 \tilde{\alpha}_V + \sigma \Lambda_2 \tilde{r}_V & -\sigma \Lambda_2 \tilde{\alpha}_U + \Lambda_1 \tilde{r}_U & \sigma \Lambda_2 \tilde{\alpha}_Q - \Lambda_1 \tilde{r}_Q & 0 \end{pmatrix},$$

$$\mathbf{M}_4 = \frac{2}{\Theta}$$
$$\times \begin{pmatrix} (\tilde{\alpha}^2 + \tilde{r}^2)/2 & \tilde{\alpha}_V \tilde{r}_U - \tilde{\alpha}_U \tilde{r}_V & \tilde{\alpha}_Q \tilde{r}_V - \tilde{\alpha}_V \tilde{r}_Q & \tilde{\alpha}_U \tilde{r}_Q - \tilde{\alpha}_Q \tilde{r}_U \\ \tilde{\alpha}_U \tilde{r}_V - \tilde{\alpha}_V \tilde{r}_U & \tilde{\alpha}_Q^2 + \tilde{r}_Q^2 - (\tilde{\alpha}^2 + \tilde{r}^2)/2 & \tilde{\alpha}_Q \tilde{\alpha}_U + \tilde{r}_Q \tilde{r}_U & \tilde{\alpha}_V \tilde{\alpha}_Q + \tilde{r}_V \tilde{r}_Q \\ \tilde{\alpha}_V \tilde{r}_Q - \tilde{\alpha}_Q \tilde{r}_V & \tilde{\alpha}_Q \tilde{\alpha}_U + \tilde{r}_Q \tilde{r}_U & \tilde{\alpha}_U^2 + \tilde{r}_U^2 - (\tilde{\alpha}^2 + \tilde{r}^2)/2 & \tilde{\alpha}_U \tilde{\alpha}_V + \tilde{r}_U \tilde{r}_V \\ \tilde{\alpha}_Q \tilde{r}_U - \tilde{\alpha}_U \tilde{r}_Q & \tilde{\alpha}_V \tilde{\alpha}_Q + \tilde{r}_V \tilde{r}_Q & \tilde{\alpha}_U \tilde{\alpha}_V + \tilde{r}_U \tilde{r}_V & \tilde{\alpha}_V^2 + \tilde{r}_V^2 - (\tilde{\alpha}^2 + \tilde{r}^2)/2 \end{pmatrix}, \tag{C.11}$$

where

$$\tilde{\alpha}^2 = \tilde{\alpha}_Q^2 + \tilde{\alpha}_U^2 + \tilde{\alpha}_V^2,$$

$$\tilde{r}^2 = \tilde{r}_Q^2 + \tilde{r}_U^2 + \tilde{r}_V^2,$$

$$\Lambda_1 = \sqrt{\sqrt{\frac{1}{4}\left(\tilde{\alpha}^2 - \tilde{r}^2\right)^2 + \left(\tilde{\alpha}_Q\tilde{r}_Q + \tilde{\alpha}_U\tilde{r}_U + \tilde{\alpha}_V\tilde{r}_V\right)^2} + \frac{1}{2}\left(\tilde{\alpha}^2 - \tilde{r}^2\right)},$$

$$\Lambda_2 = \sqrt{\sqrt{\frac{1}{4}\left(\tilde{\alpha}^2 - \tilde{r}^2\right)^2 + \left(\tilde{\alpha}_Q\tilde{r}_Q + \tilde{\alpha}_U\tilde{r}_U + \tilde{\alpha}_V\tilde{r}_V\right)^2} - \frac{1}{2}\left(\tilde{\alpha}^2 - \tilde{r}^2\right)},$$

$$\Theta = \Lambda_1^2 + \Lambda_2^2,$$

$$\sigma = \text{sign}\left(\tilde{\alpha}_Q\tilde{r}_Q + \tilde{\alpha}_U\tilde{r}_U + \tilde{\alpha}_V\tilde{r}_V\right), \tag{C.12}$$

and where the tilde quantities $\tilde{\alpha}_X$, $\tilde{r}_X$ take into account the basis rotation by an angle χ and read

$$\begin{pmatrix} \tilde{\alpha}_Q \\ \tilde{\alpha}_U \end{pmatrix} = \begin{pmatrix} \cos 2\chi & -\sin 2\chi \\ \sin 2\chi & \cos 2\chi \end{pmatrix} \begin{pmatrix} \alpha_Q \\ \alpha_U \end{pmatrix}, \tag{C.13}$$

and similarly for $\tilde{r}_Q$ and $\tilde{r}_U$, while $\tilde{\alpha}_{I,V}$ and $\tilde{r}_V$ are the same as their counterparts without a tilde, given that I and V are not affected by the rotation.

ORCID iDs

N Aimar ⓘ https://orcid.org/0000-0001-5710-452X
T Paumard ⓘ https://orcid.org/0000-0003-0655-0452
F H Vincent ⓘ https://orcid.org/0000-0002-9214-0830
E Gourgoulhon ⓘ https://orcid.org/0000-0001-5156-6096
G Perrin ⓘ https://orcid.org/0000-0003-0680-0167

References

Aimar N, Dmytriiev A, Vincent F H, El Mellah I, Paumard T, Perrin G and Zech A 2023 *Astron. Astrophys.* **672** A62
Event Horizon Telescope Collaboration *et al* 2019 *Astrophys. J.* **875** L5
Anantua R, Ressler S and Quataert E 2020 *Mon. Not. R. Astron. Soc.* **493** 1404–18
Broderick A E, Fish V L, Johnson M D, Rosenfeld K, Wang C, Doeleman S S, Akiyama K, Johannsen T and Roy A L 2016 *Astrophys. J.* **820** 137
Bronzwaer T, Davelaar J, Younsi Z, Mościbrodzka M, Falcke H, Kramer M and Rezzolla L 2018 *Astron. Astrophys.* **613** A2
Bronzwaer T, Younsi Z, Davelaar J and Falcke H 2020 *Astron. Astrophys.* **641** A126
Cárdenas-Avendaño A and Lupsasca A 2023 *Phys. Rev.* D **108** 064043
Cárdenas-Avendaño A, Lupsasca A and Zhu H 2023 *Phys. Rev.* D **107** 043030
Casse F, Varniere P and Meliani Z 2017 *Mon. Not. R. Astron. Soc.* **464** 3704–12
Chael A, Narayan R and Johnson M D 2019 *Mon. Not. R. Astron. Soc.* **486** 2873–95
Chael A, Rowan M, Narayan R, Johnson M and Sironi L 2018 *Mon. Not. R. Astron. Soc.* **478** 5209–29
Chan C k, Medeiros L, Özel F and Psaltis D 2018 *Astrophys. J.* **867** 59
Chan C k, Psaltis D, Özel F, Medeiros L, Marrone D, Sadowski A and Narayan R 2015 *Astrophys. J.* **812** 103
Dauser T, Wilms J, Reynolds C S and Brenneman L W 2010 *Mon. Not. R. Astron. Soc.* **409** 1534–40
Davelaar J, Mościbrodzka M, Bronzwaer T and Falcke H 2018 *Astron. Astrophys.* **612** A34
Dexter J 2016 *Mon. Not. R. Astron. Soc.* **462** 115–36

Dexter J *et al* 2020 *Mon. Not. R. Astron. Soc.* **497** 4999–5007

Dexter J and Agol E 2009 *Astrophys. J.* **696** 1616–29

Dovčiak M, Muleri F, Goosmann R W, Karas V and Matt G 2008 *Mon. Not. R. Astron. Soc.* **391** 32–38

Dovčiak M, Papadakis I E, Kammoun E S and Zhang W 2022 *Astron. Astrophys.* **661** A135

Event Horizon Telescope Collaboration *et al* 2022 *Astrophys. J.* **930** L12

Gelles Z, Himwich E, Johnson M D and Palumbo D C M 2021 *Phys. Rev.* D **104** 044060

Gralla S E, Holz D E and Wald R M 2019 *Phys. Rev.* D **100** 024018

Gralla S E, Lupsasca A and Marrone D P 2020 *Phys. Rev.* D **102** 124004

Gralla S E, Lupsasca A and Strominger A 2018 *Mon. Not. R. Astron. Soc.* **475** 3829–53

GRAVITY Collaboration *et al* 2018 *Astron. Astrophys.* **618** L10

GRAVITY Collaboration *et al* 2020 *Astron. Astrophys.* **635** A143

GRAVITY Collaboration *et al* 2023 *Astron. Astrophys.* **677** L10

Grould M, Vincent F H, Paumard T and Perrin G 2017 *Astron. Astrophys.* **608** A60

Hamaker J P and Bregman J D 1996 *Astron. Astrophys. Suppl. Ser.* **117** 161–5

Himwich E, Johnson M D, Lupsasca A and Strominger A 2020 *Phys. Rev.* D **101** 084020

Huang L, Liu S, Shen Z Q, Yuan Y F, Cai M J, Li H and Fryer C L 2009 *Astrophys. J.* **703** 557–68

Huang L and Shcherbakov R V 2011 *Mon. Not. R. Astron. Soc.* **416** 2574–92

Jiménez-Rosales A *et al* 2021 *Mon. Not. R. Astron. Soc.* **503** 4563–75

Krawczynski H *et al* 2022 *Science* **378** 650–4

Landi Degl'Innocenti E and Landi Degl'Innocenti M 1985 *Sol. Phys.* **97** 239–50

Marszewski A, Prather B S, Joshi A V, Pandya A and Gammie C F 2021 *Astrophys. J.* **921** 17

Mignon-Risse R, Aimar N, Varniere P, Casse F and Vincent F 2021 *SF2A-2021: Proc. Annual Meeting of the French Society of Astronomy and Astrophysics* ed A Siebert, K Baillié, E Lagadec, N Lagarde, J Malzac, J B Marquette, M N'Diaye, J Richard and O Venot pp 113–6

Misner C W, Thorne K S and Wheeler J A 1973 *Gravitation* (Freeman)

Mościbrodzka M, Falcke H and Shiokawa H 2016 *Astron. Astrophys.* **586** A38

Mościbrodzka M and Gammie C F 2018 *Mon. Not. R. Astron. Soc.* **475** 43–54

Nalewajko K, Sikora M and Różańska A 2020 *Astron. Astrophys.* **634** A38

Noble S C, Leung P K, Gammie C F and Book L G 2007 *Class. Quantum Grav.* **24** S259–74

Page D N and Thorne K S 1974 *Astrophys. J.* **191** 499–506

Pihajoki P, Mannerkoski M, Nättilä J and Johansson P H 2018 *Astrophys. J.* **863** 8

Porth O, Mizuno Y, Younsi Z and Fromm C M 2021 *Mon. Not. R. Astron. Soc.* **502** 2023–32

Prather B S *et al* (Event Horizon Telescope Collaboration) 2023 *Astrophys. J.* **950** 35

Pu H Y, Yun K, Younsi Z and Yoon S J 2016 *Astrophys. J.* **820** 105

Rybicki G B and Lightman A P 1979 *Radiative Processes in Astrophysics* (Wiley)

Shcherbakov R V 2008 *Astrophys. J.* **688** 695–700

Transactions of the International Astronomical Union 1973 *Trans. Int. Astron. Union* **15** 165–7

Varniere P, Casse F and Vincent F H 2018 *SF2A-2018: Proc. Annual Meeting of the French Society of Astronomy and Astrophysics* ed P Di Matteo, F Billebaud, F Herpin, N Lagarde, J B Marquette, A Robin and O Venot p Di

Vincent F H, Abramowicz M A, Zdziarski A A, Wielgus M, Paumard T, Perrin G and Straub O 2019 *Astron. Astrophys.* **624** A52

Vincent F H, Paumard T, Gourgoulhon E and Perrin G 2011 *Class. Quantum Grav.* **28** 225011

Vincent F H, Wielgus M, Aimar N, Paumard T and Perrin G 2023 arXiv:2309.10053

Vos J, Mościbrodzka M A and Wielgus M 2022 *Astron. Astrophys.* **668** A185

Walker M and Penrose R 1970 *Commun. Math. Phys.* **18** 265–74

Westfold K C 1959 *Astrophys. J.* **130** 241

White C J 2022 *Astrophys. J. Suppl. Ser.* **262** 28

Wielgus M, Moscibrodzka M, Vos J, Gelles Z, Martí-Vidal I, Farah J, Marchili N, Goddi C and Messias H 2022 *Astron. Astrophys.* **665** L6

Xiao-lin Y, Jian-cheng W, Chu-yuan Y and Zun-li Y 2021 *Astrophys. J. Suppl. Ser.* **254** 29

Younsi Z, Porth O, Mizuno Y, Fromm C M and Olivares H 2020 *Perseus in Sicily: From Black Hole to Cluster Outskirts* vol 342, ed K Asada, E de Gouveia Dal Pino, M Giroletti, H Nagai and R Nemmen (Cambridge University Press) pp 9–12